HEDL-SA-1300FP

CONF-771107--97

INTERSUBASSEMBLY INCOHERENCIES AND GROUPING TECHNIQUES IN LMFBR HYPOTHETICAL OVERPOWER ACCIDENT

MASTER

N. P. Wilburn
Hanford Engineering Development Laboratory
Richland, Washington 99352

October 1977

For Presentation at the American Nuclear Society 1977 Winter Meeting in San Francisco, California, November 27-December 2, 1977

INTERSUBASSEMBLY INCOHERENCIES AND GROUPING TECHNIQUES IN LMFBR HYPOTHETICAL OVERPOWER ACCIDENT

N. P. Wilburn

I. INTRODUCTION

Safety studies for postulated unprotected transient overpower (TOP) and loss-of-flow (LOF) accidents in an LMFBR system have generally employed integrated multi-channel coupled neutronics, thermal-hydraulic computer codes, such as SAS3A or MELT-III. Because of the complexity of these codes, large amounts of computer time are required, which are roughly proportionate to the number of channels used in the simulation. Therefore, there is strong incentive to use as few channels (wherein a group of subassemblies is represented by a single pin in a cylindrical geometry) as possible in a study. When a single channel is used to represent several subassemblies, the assumption is made that all pins in all subassemblies behave coherently. However, it was recognized that complete coherent behavior could not be expected due to the differences that exist between the various subassemblies which make up a given channel, such as power, power profile, effective burnup, power to flow, and several other parameters. It was also recognized that there were intrasubassembly differences expected between pins in each subassembly caused by: 1) the skewing of the power profile across the subassembly, 2) the influence of the subassembly can upon the outer rows of pins, and 3) flow area variations between subchannels. These three effects lead to differing axial temperature distributions across the subchannels of the subassembly.

The first purpose of this paper is to investigate the behavior of two Fast Test Reactor (FTR) cores: the beginning-of-cycle-4 (BOC-4) and end-of-cycle-4 (EOC-4) cores under a hypothetical TOP accident, in order to estimate the intersubassembly incoherencies, and the effect that these incoherencies have on the scenario of the TOP accident. The effects of failure incoherencies in an LMFBR overpower accident have been investigated previously wherein the subassembly behaviors were combined in a stochastic fashion. However, in this report, the technique is to represent the core by one subassembly per channel in which a single pin in cylindrical geometry represents all of the 217 pins in a given subassembly using the MELT-IIIA code. The MELT-IIIA code has the

capability of modeling up to 100 channels, and with appropriate changes in FORTRAN DIMENSION statements, as many channels as required for a given analysis may be used.

In a companion paper, the subject of the intrasubassembly incoherencies under TOP accident conditions will be considered. The COBRA-III/MELT code will be used to investigate failure sequences and then the effect of such failures upon the subassembly coolant behavior. In this companion paper, the effect of a deterministic sequence of pin failures due to the influence of the varying temperature distribution across a subassembly will be investigated, as well as the effects of stochastic failures based on the failure model statistics.

In this paper, a subassembly is still represented by a single pin in cylindrical geometry. The particular cases that have been chosen are the base case, which was used previously, where the BOC-4 core for the FTR was studied. Also the EOC-4 case will be investigated. The 3DB series of codes was used to obtain power profiles, fuel, sodium, and steel worth curves and Doppler weighting coefficients in the same way as before. For these two cores (BOC-4 and EOC-4) 76-channel runs in which each driver assembly was represented by a single channel were made using the MELT-IIIA code system for 0.5$/sec ramps and 1$/sec ramps, and the results are presented.

The second purpose of this paper is to determine a more effective means to group subassemblies into a lesser number of channels for TOP HCDA analysis using the results from the 76-channel runs. In doing this, the purpose is to determine what criteria seem to be the most important in grouping. A method previously employed was to first group the subassemblies approximately according to power levels and burnups into as many channels as the code permitted; then, secondly, to make computer runs using a failure criteria to determine the channel failure sequence; and finally, using this failure sequence information, regroup into smaller numbers of channels and rerun. Even though significant differences begin to accrue for the longer time scales, the results show nearly identical results up to and even beyond initial neutronic shutdown. The assumption was made, however, that the 20-channel representation was an accurate description of the behavior of the core.

In this paper, the new grouping method is established, and the important criteria are described. The applicability of the resultant grouping is

investigated for two ramp rates and for two different failure criteria in order to determine the breadth of the grouping applicability.

A final purpose of this paper is to compare the results of this new grouping method and those obtained from the former grouping method with the results of 76-channel runs. In particular, it will be shown that the base case 20-channel grouping used leads to ultimate reactivity values which differ from the 76-channel values by as much as 1$.

II. 76-CHANNEL RESULTS

The 76-driver subassemblies in the FTR BOC-4 and EOC-4 cores have been represented by 76 channels in the MELT-IIIA code. The channel identification of the individual subassemblies are shown in Figure 1 where a core map of the FTR is presented. The numbering system is arbitrary, starting with the left-hand side of the figure and moving vertically and then horizontally toward the right. The direction of numbering corresponds to the direction used in the 3DB document. However, in that document the special test assemblies and the control rods were also numbered.

Figure 2 shows the total power in the subassemblies for each of the 76-driver assemblies. Figure 3 shows the peak burnup of the individual subassemblies for the BOC-4 FTR core in megawatt days/Kg. As can be seen, there are some 23 subassemblies having zero burnup. In the MELT-IIIA analyses, these subassemblies are assumed not to fail during the course of a hypothetical, unprotected transient overpower accident because of the greater ductility of the cladding. There is some question as to when these channels become better described by a burned pin than by a zero burnup pin during the course of cycle 4, as discussed below.

Figure 4 illustrates the restructuring as predicted by the SIEX subroutine of the MELT code. The restructuring is shown in a nodal fashion in which the 11 radial nodes and 18 axial nodes used in the MELT code give a discreet restructuring as opposed to the continuous restructuring calculation carried on in the SIEX code. The assumption is made in calculation of the BOC-4 core restructuring that the axial power profile for the subassembly at the time of the beginning of cycle 4 is identical to that which existed when the subassembly was first inserted into the core. However, the critical areas of restructuring in the failure models are above the center line of the subassembly and in the region the power profiles are almost identical. The restructuring

plot in Figure 4 demonstrates quite well the effects of the control rod shadowing (note the four subassemblies at the lower part of the figure). The influence of the control rods (assumed to be halfway inserted during the 3DB calculation) is seen in the pushed-down effect upon the restructuring in the vicinity of the rods.

The four cases run for this study with the 76-channel representation of the FTR core are:

- A 0.5$/sec ramp in the BOC-4 core using the "Failure Potential" fuel pin failure model.
- A 1$/sec ramp in the BOC-4 core using the Failure Potential.
- A 0.5$/sec ramp in the EOC-4 core using the Failure Potential.
- A 0.5$/sec ramp in the BOC-4 core using the Damage Parameter Failure criteria.

Results of these runs will be described below and in Figures 5 through 19.

Figure 5 illustrates the failure sequence by subassembly for the 0.5$/sec ramp in the BOC-4 core using the Failure Potential. Figure 6 shows the failure sequence by subassembly for the BOC-4 core with a 1$/sec ramp using the Failure Potential, while Figure 7 shows the failure sequence by subassembly for the EOC-4 core with a 0.5$/sec ramp and the Failure Potential. Figure 8 demonstrates the number of subassemblies predicted to fail as a function of time for the BOC-4 core with a 0.5$/sec ramp using the Failure Potential, as does Figure 9 for the BOC-4 core using the 1$/sec ramp with the Failure Potential, and Figure 10 for the EOC-4 core with a 0.5$/sec ramp and the Failure Potential. In addition to other information to be described later, Figure 11 shows the failure sequence for the 76-channel run for a 0.5$/sec ramp using the Damage Parameter Failure criteria. Figures 12 through 15 illustrate the net reactivities for these same four cases, while Figures 16 through 19 show the corresponding power as a function of time for these four 76-channel cases.

As can be seen in all these cases, after a very few tenths of a second the reactor is strongly shut down by a negative reactivity of several dollars. This shutdown is due to the high failure locations predicted by the Damage Parameter and the Failure Potential models, and the initial fuel motion out of

the pins to this location. This location of failure has been shown not to deviate very much throughout a large range of statistical variations applied to the model. The power, after the initial failures predicted by these models, comes down very rapidly to below the steady-state value.

A question has been raised about the status of the subassemblies containing fresh pins during the course of the transient. It has been demonstrated by experimental evidence that the failure mechanism of a fresh pin is by coolant boiling followed shortly by cladding dryout and cladding melting. The question, then, is how close to this latter failure condition do the subassemblies containing fresh pins come during the course of a transient overpower accident in a beginning-of-cycle-4 core. Figure 20 is presented to answer this question. The coolant temperature shown is that existing in the topmost axial node of the core (which has the highest temperature occurring in the coolant) for channel 38 of the 76-channel run. As shown in Figures 1 and 2, the peak power in this subassembly is relatively high compared to the rest of the reactor, and it is the highest of the zero burnup subassemblies. The saturated temperature plotted in this figure corresponds to the pressure considered in the node. As can be seen, the coolant temperature never reaches saturation as predicted by the MELT code. The rapid variability of the saturation temperature is due directly to the successive failures occurring in other subassemblies. These in turn affect the plenum pressures and hence the pressures throughout an individual subassembly. Momentary coolant saturation temperatures might be reached, but in all cases these would exist for only a few milliseconds, so it would not be possible for cladding dryout followed by melting and failure to occur.

Figure 21 is presented to illustrate the subassembly failure sequences for the three runs using the Failure Potential as a function of the peak burnup present in the subassembly. Also shown in Figure 21 is the range of experimental data obtained from the TREAT reactor which was used in the fitting of the Failure Potential Model. As can be seen, a large number of early failures in all three runs occur in subassemblies which have a peak burnup of about 20 megawatt days/Kg.

It should be noted also that there are some 51 subassemblies in the BOC-4 core having a peak burnup less than the minimum value of burnup used in the range of the experimental data in fitting this Failure Potential Model. In the case of the EOC-4 core, there are 27 subassemblies having a peak burnup less than the minimal experimental values.

In the BOC-4 core there are 23 subassemblies having zero burnup. The standard procedure using the MELT code is simply to forbid a failure in a channel having zero burnup, since the failure would presumably be by boiling followed by the cladding dryout and failure, and, as seen in Figure 20, it is presumed that the boiling does not occur in these subassemblies. However, during the course of cycle 4, as the core proceeds from the beginning to the end of cycle conditions, there is the question regarding what situation is most descriptive of the reactor, and what should be used as the base case. As shown in Figures 2, 3 and 4, which illustrate the failure sequences for the BOC-4 and EOC-4 cores as a function of ramp rate and position in the core, the subassemblies turned off due to being zero burnup in the BOC-4 core enter into the early failures of the EOC-4 core. The question then arises as to when the fresh subassemblies influence the course of events in an unprotected HCDA TOP accident. It is presumed that a base case, representative of a core somewhere midway between the BOC-4 and EOC-4 core, would probably be more representative of the average conditions throughout cycle 4.

III. GROUPING OF FTR SUBASSEMBLIES INTO 7 CHANNELS

In the analysis of the transient overpower accident by either the SAS3A or MELT-III codes, the subassemblies constituting the reactor are grouped into channels where several subassemblies are represented by a single channel. The behavior of all pins involved was modeled by a single pin in cylindrical geometry. The method previously employed was, first to group the subassemblies approximately according to power level and burnup pattern into as many channels as the code permitted. In the case of SAS3A this was 10 channels and in MELT it was 20 channels. A computer run was then made using a Failure Criteria and this subassembly grouping to determine the failure sequence of the channels. Then, using this failure sequence information, the channels were grouped into a smaller number by assuming that channels which failed at approximately the same time exhibited like characteristics and, thus, could be grouped together. This procedure was used in the analysis of the FFTF for the transient overpower accident. However, it was shown that even though the scenario was basically the same in all cases for a 2-, 4-, 7-, 10-, or 20-channel run, there was a wide degree of variation in the accident description details.

With the advent of the MELT code's larger number of channels, it was possible to do an analysis of the complete reactor using one subassembly per

channel as described above, and then to use this information in more adequately grouping the subassemblies. When a 76-channel analysis was performed and when the subassemblies were ordered in a tabular fashion by their failure sequence, certain parameters were found to be important to the failure sequence. These parameters, in order of their importance when establishing a channel grouping, were found to be as follows:

- fresh or burned pin,
- total subassembly power,
- individual axial nodal power values above core midplane,
- subassembly power to flow ratio,
- burnup.

A specialized "least squares" program was written to determine the grouping of subassemblies. This program minimized the sum of the weighted mean-square variations of these parameters between the subassemblies making up a channel. Parameter weights, parameters, and number of channels are input. This program was then used for making groupings of 20-, 10-, and 7-channel runs in the FFTF for the BOC-4 core.

Upon making runs with these groupings, it was determined that a 7-channel representation of the FTR core was adequately descriptive of the results obtained when the core was modeled with a 76-channel run. Table I shows the groupings of subassemblies expected to fail early into three channels of the 7-channel run. The table presents the range and average values across the set of subassemblies making up a channel, and the 7-channel value obtained when the MELT calculation was carried out. As can be seen, the variation of most of the parameters, with the exception of the peak burnup, is fairly small in terms of percent. The peak burnup, however, in one or two subassemblies making up the group varies markedly from the average. However, the procedure of taking the extreme values and eliminating them from the average was applied here in making up a 7-channel representation of the reactor.

The particular subassemblies which make up the 7-channel run are shown in Figure 22 where a different legend is used for each channel. Figures 23, 24 and 25 show the microstructure variation across the subassemblies which make up the particular channel. As can be seen, the variation is minimal. Since

the microstructure with the associated power profile and fission product gas release are the more important parameters of the Failure Potential Model, one would expect a small variation in failure times. As shown in Table I, this is proved to be the case.

Figures 26, 27 and 28 show the subassembly spread and 7-channel value for the axial power profiles of these three channels. Again, this spread is fairly minimal. MELT was used to run this 7-channel case for the same set of runs on the BOC-4 core used in the 76-channel case. The results for the numbers of subassemblies failing as a function of time are compared in Figures 8, 9, and 11. As shown, the failure sequence tracks the 76-channel runs fairly closely, both as far as number of subassemblies failing, and the times of failure for the two ramps involved, (0.5$/sec and 1$/sec) and the two failure criteria (the Damage Parameter and Failure Potential).

Figures 12, 13 and 14 show the behavior of the net reactivity for these three runs. The net reactivity of each 7-channel run tracks the 76-channel run very closely. Finally, the power profiles are shown for the same three runs in Figures 16, 17 and 19.

For a comparison of the current channel-grouping method compared with the former method, the reader is referred to Figures 11, 15 and 19. In these figures the subassemblies failing, net reactivity, and power profiles are shown for the Damage Parameter Failure criteria of a 0.5$/sec TOP ramp. The 20-channel case presented here is the original transient overpower base case described in Reference 7. Due to the differences in failure sequences of the channels making up the 20-channel run, there is a pronounced bump after the initial failure, both in the reactivity plots and in the power plots. Also, it should be noted that the net reactivity after a substantial time subsequent to failure is approximately a dollar more negative in the case of the original 20-channel base case compared with the 76-channel representation and the 7-channel case method of grouping.

IV. CONCLUSIONS

It was the purpose of this paper to consider a much more detailed analysis of the FTR core using the 100-channel MELT-IIIA code. Results were studied for the transient overpower accident (where 0.5$/sec and 1$/sec ramps) and in which the Damage Parameter and the Failure Potential criteria were used. Using the information obtained from these series of runs, a new method of

grouping the subassemblies into channels has been developed. Also, it was demonstrated that a 7-channel representation of the FTR core using this method does an adequate job of representing the behavior during a hypothetical disruptive transient overpower core accident.

It has been shown that this new 7-channel grouping method does a better job than the original 20-channel grouping used for the base case in Reference 7. It has also been demonstrated that the incoherency effects between subassemblies as shown during the 76-channel representation of the reactor can be adequately modeled by 7-channels, provided the 7-channels are selected according to the criteria stated in this report. The overall results of power and net reactivity were shown to be only slightly different in the two cases of the 7-channel and the 76-channel runs. Therefore, it can be concluded that any intersubassembly incoherencies can be modeled adequately by a small number of channels, provided the subassemblies making up these channels are selected according to the criteria stated.

However, it remains to be seen whether the effects of intrasubassembly incoherencies will have a more marked effect. The known, large temperature variations and power skew across an individual subassembly certainly will affect the failure times of the various pins in the subassembly. Consequently, the fuel motion in the subassembly will vary from that calculated for an average pin representing the total subassembly. The net results of this intrasubassembly incoherence cannot be known until substantial modifications are made to either the SAS or MELT codes in which failure times for times for individual subgroupings of pins making up a single channel can be modeled. The SAS code allows for subgroupings, but it does not allow for individual calculation of failure times for these subgroupings. The difference in failure times is put in simply as a parameter with respect to the failure time of the first pins to fail.

Table I
Comparison of 76- vs. 7-Channel Parameters and Results

CHANNEL		1	2	3	4	5	6	7	RANGE(W/O*)	AVERAGE(W/O*)	7-CHANNEL VALUE
	76 Channel I.D./Ring	29/2	39/1	47/2	--	--	--	--	--	--	--
	Peak Power (Kw/ft)	12.16	11.92	12.26	--	--	--	--	.34	12.11	12.11
	Peak Burnup (MWD/Kg)	20.5	40.9*	20.7	--	--	--	--	20.4 (.2)	27.4 (20.6)	20.6
	Power/Flow	1.446	1.421	1.456	--	--	--	--	.035	1.441	1.439
	S.S. Plenum Pressure (Bars)	9.113	8.429*	9.218	--	--	--	--	.789 (.105)	8.92 (9.166)	9.117
1	S.S. Fission Gas Released (cc)	24.33	20.57*	24.94	--	--	--	--	4.37 (.61)	23.28 (24.64)	24.42
	D.P. Failure (0.5$/sec) Node	23	23	23	--	--	--	--	0	23	23
	D.P. Failure (0.5$/sec) Time	2.6390	2.6335	2.6290	--	--	--	--	.0100	2.6338	2.6395
	F.P. Failure (0.5$/sec) Node	23	22	23	--	--	--	--	1	22-23	23
	F.P. Failure (0.5$/sec) Time	3.1100	3.1160	3.1005	--	--	--	--	.0155	3.1088	3.1140
	F.P. Failure (1.0$/sec) Node	22	22	22	--	--	--	--	0	22	22
	F.P. Failure (1.0$/sec) Time	1.7075	1.6990	1.7030	--	--	--	--	.0085	1.7032	1.7140
	76 Channel I.D./Ring	22/3	28/3	31/3	40/3	46/3	49/3	55/3	--	--	--
	Peak Power (Kw/ft)	10.72	10.98	11.40	10.92	10.93	11.44	11.09	.72	11.07	11.07
	Peak Burnup (MWD/Kg)	37.1	37.7	19.5*	38.0	37.7	19.6*	38.5	19.0 (1.4)	32.6 (37.8)	37.8
	Power/Flow	1.513	1.540	1.608	1.541	1.534	1.616	1.555	.103	1.558	1.557
	S.S. Plenum Pressure (Bars)	14.282	14.648	8.429*	14.852	14.620	8.429*	15.099	6.67 (.817)	12.908 (14.700)	14.885
2	S.S. Fission Gas Released (cc)	62.93	65.10	20.57*	66.53	64.99	20.92*	68.04	47.47 (5.11)	52.73 (65.52)	66.48
	D.P. Failure (0.5$/sec) Node	22	22	22	22	22	22	22	0	22	22
	D.P. Failure (0.5$/sec) Time	2.7155	2.7030	2.7060	2.7200	2.7060	2.7140	2.7100	.0170	2.7106	2.7150
	F.P. Failure (0.5$/sec) Node	23	22	22	23	22	23	23	1	22-23	23
	F.P. Failure (0.5$/sec) Time	3.2465	3.2150	3.1860	3.2150	3.2225	3.1760	3.2115	.0705	3.2104	3.2130
	F.P. Failure (1.0$/sec) Node	21	21	22	21	21	21	21	0	21	21
	F.P. Failure (1.0$/sec) Time	1.7545	1.7470	1.7400	1.7470	1.7505	1.7395	1.7400	.0150	1.7455	1.7430
	76 Channel I.D./Ring	20/4	32/4	42/5	57/5	59/5	61/4	62/4	--	--	--
	Peak Power (Kw/ft)	10.52	10.64	10.36	10.93	10.51	10.66	10.18	.75	10.54	10.55
	Peak Burnup (MWD/Kg)	17.7	18.2	17.6	19.5	18.1	18.2	17.8	1.9	18.2	18.2
	Power/Flow	1.240	1.255	1.281	1.334	1.302	1.253	1.187	.147	1.265	1.237
	S.S. Plenum Pressure (Bars)	7.497	7.652	7.481	8.036	7.663	7.633	7.252	.784	7.602	7.597
3	S.S. Fission Gas Released (cc)	15.25	16.20	14.72	18.08	15.80	16.09	14.05	4.03	15.74	15.72
	D.P. Failure (0.5$/sec) Node	21	21	21	21	21	21	--	0	21	21
	D.P. Failure (0.5$/sec) Time	2.8240	2.8185	2.7710	2.7200	2.7545	2.8225	--	.1040	2.7851	2.7870
	F.P. Failure (0.5$/sec) Node	--	--	22	22	22	--	--	0	22	22
	F.P. Failure (0.5$/sec) Time	--	--	3.3100	3.2570	3.2755	--	--	.0530	3.2808	3.3530
	F.P. Failure (1.0$/sec) Node	21	21	21	21	21	21	--	0	21	21
	F.P. Failure (1.0$/sec) Time	1.8080	1.8005	1.7955	1.7715	1.7840	1.7970	--	.0365	1.7928	1.8010

* NOTE: Subassemblies deleted from averages noted (W/O*)

LEGEND

SR	SAFETY ROD
CR	CONTROL ROD
MT	MATERIAL TEST
SP	SPECIAL PURPOSE TEST
GP	GENERAL PURPOSE CLOSED LOOP TEST
PSR	PERIPHERAL SHIM ROD
NN	76-CHANNEL IDENTIFICATION

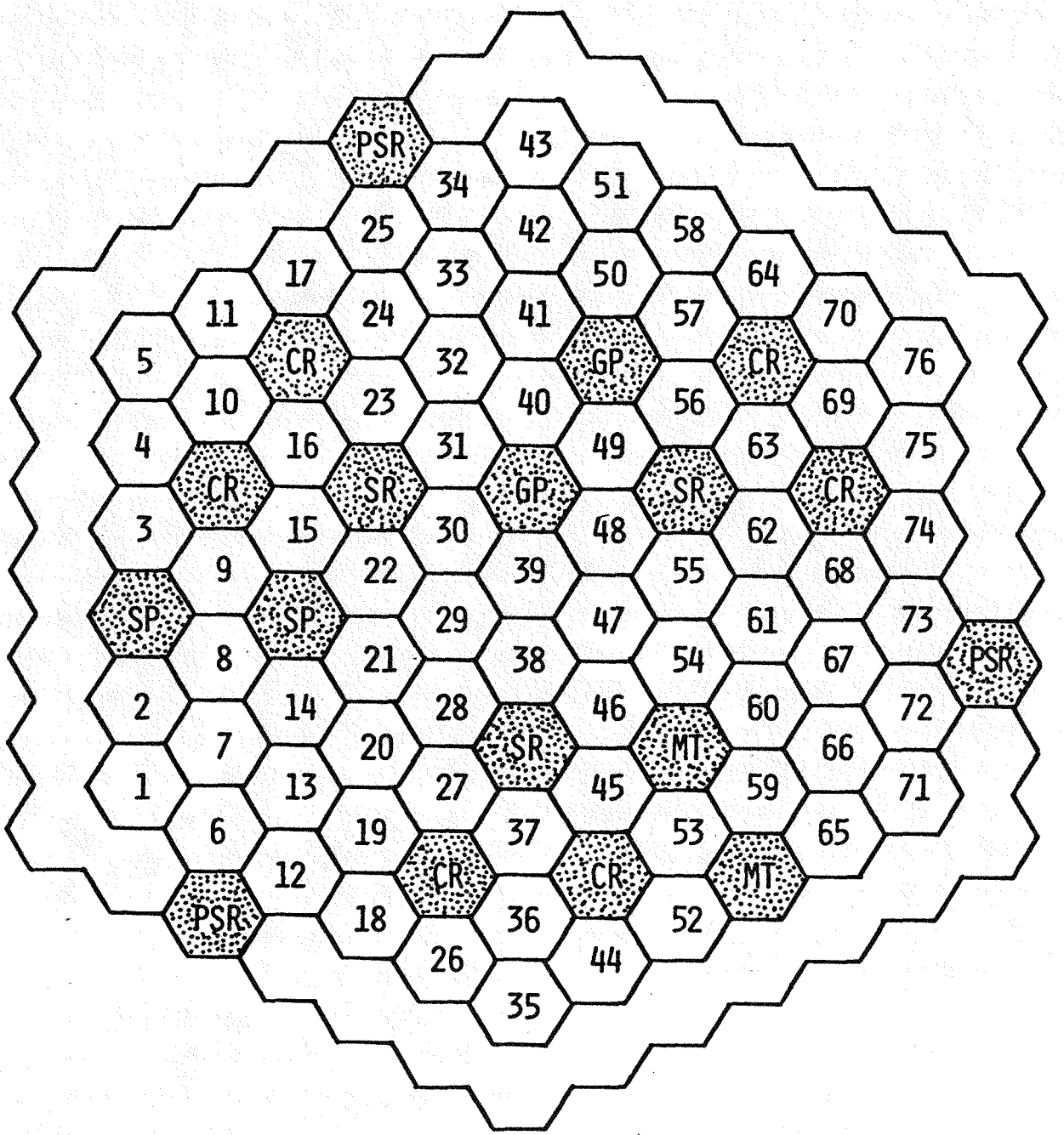

FIGURE 1. 76-Channel Representation of Subassemblies. HEDL P60422-16

LEGEND

SR	SAFETY ROD
CR	CONTROL ROD
MT	MATERIAL TEST
SP	SPECIAL PURPOSE TEST
GP	GENERAL PURPOSE CLOSED LOOP TEST
PSR	PERIPHERAL SHIM ROD
N.NN	TOTAL POWER (MW)

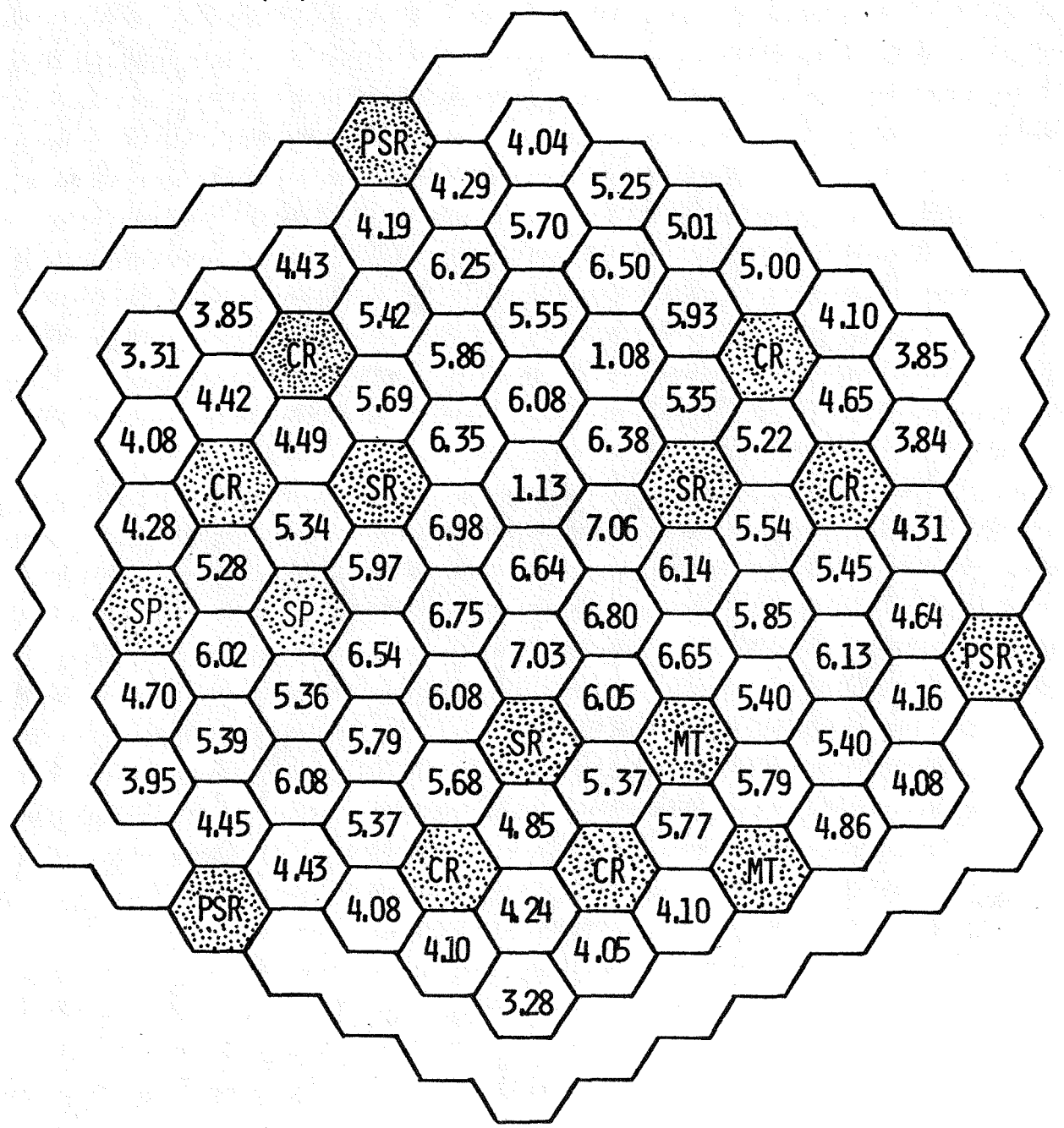

FIGURE 2. Subassembly Power -- BOC-4 Core. HEDL P00422-17

LEGEND

SR	SAFETY ROD
CR	CONTROL ROD
MT	MATERIAL TEST
SP	SPECIAL PURPOSE TEST
GP	GENERAL PURPOSE CLOSED LOOP TEST
PSR	PERIPHERAL SHIM ROD
NN.N	PEAK BURNUP (MWD/KG)

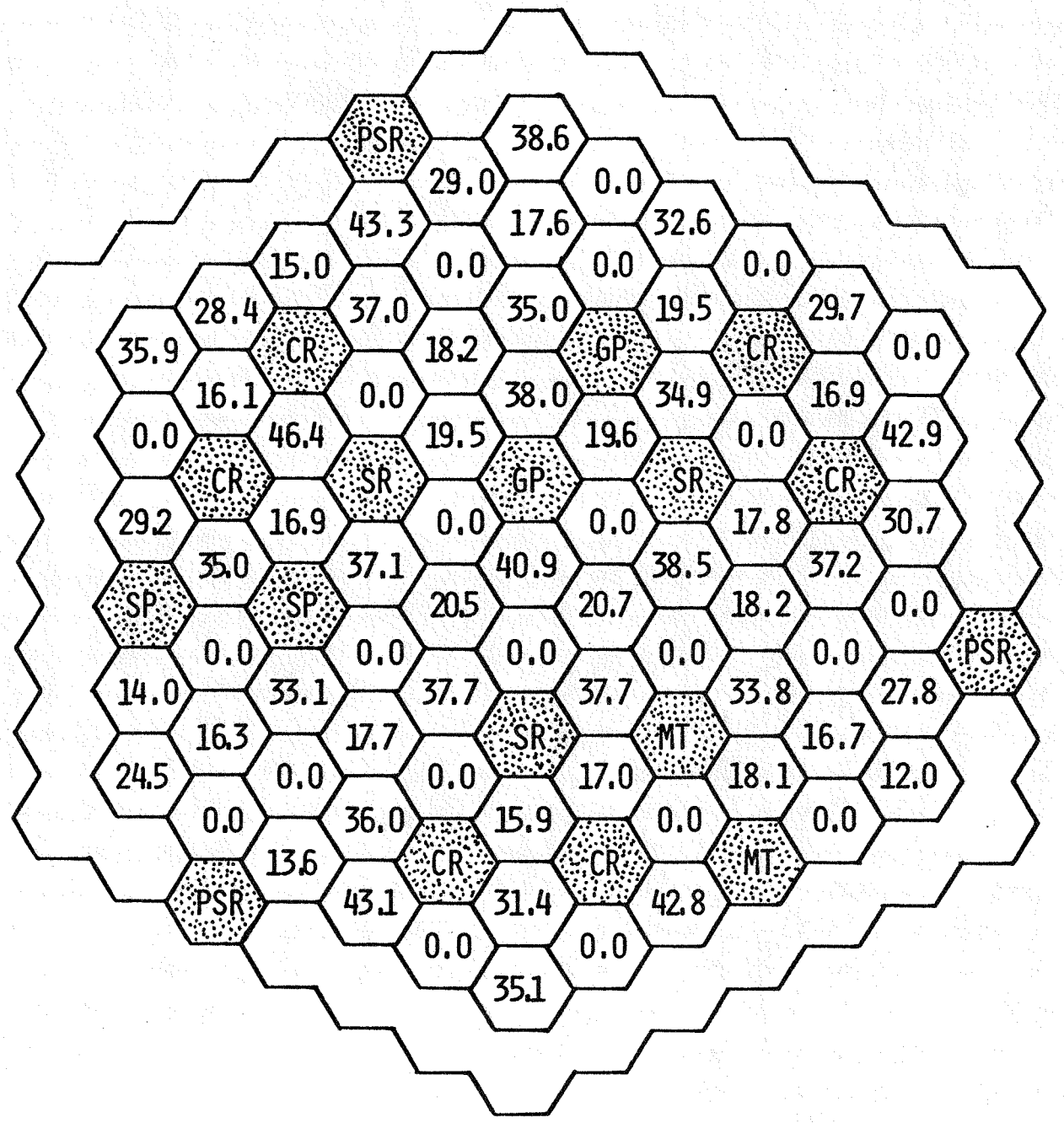

FIGURE 3. Subassembly Burnup -- BOC-4 Core. HEDL P00422-9

FIGURE 4. Subassembly Restructuring -- BOC-4 Core.

LEGEND

SR	SAFETY ROD
CR	CONTROL ROD
MT	MATERIAL TEST
SP	SPECIAL PURPOSE TEST
GP	GENERAL PURPOSE CLOSED LOOP TEST
PSR	PERIPHERAL SHIM ROD
NN	FAILURE SEQUENCE

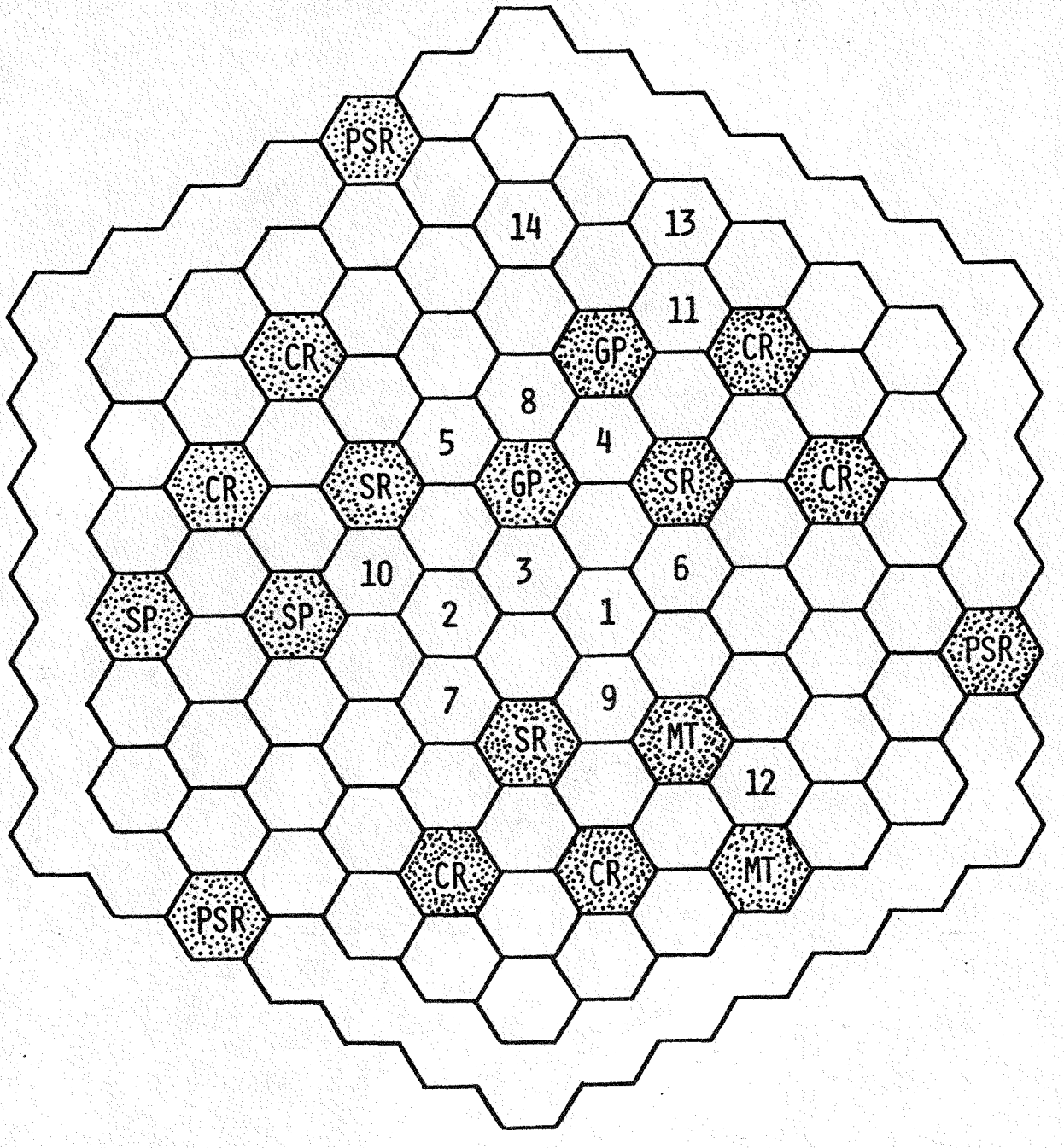

FIGURE 5. BOC-4 Subassembly Failure Sequence (0.5$/sec TOP)-Failure Potential Model.

HEDL P00422-23

LEGEND

SR	SAFETY ROD
CR	CONTROL ROD
MT	MATERIAL TEST
SP	SPECIAL PURPOSE TEST
GP	GENERAL PURPOSE CLOSED LOOP TEST
PSR	PERIPHERAL SHIM ROD
NN	FAILURE SEQUENCE

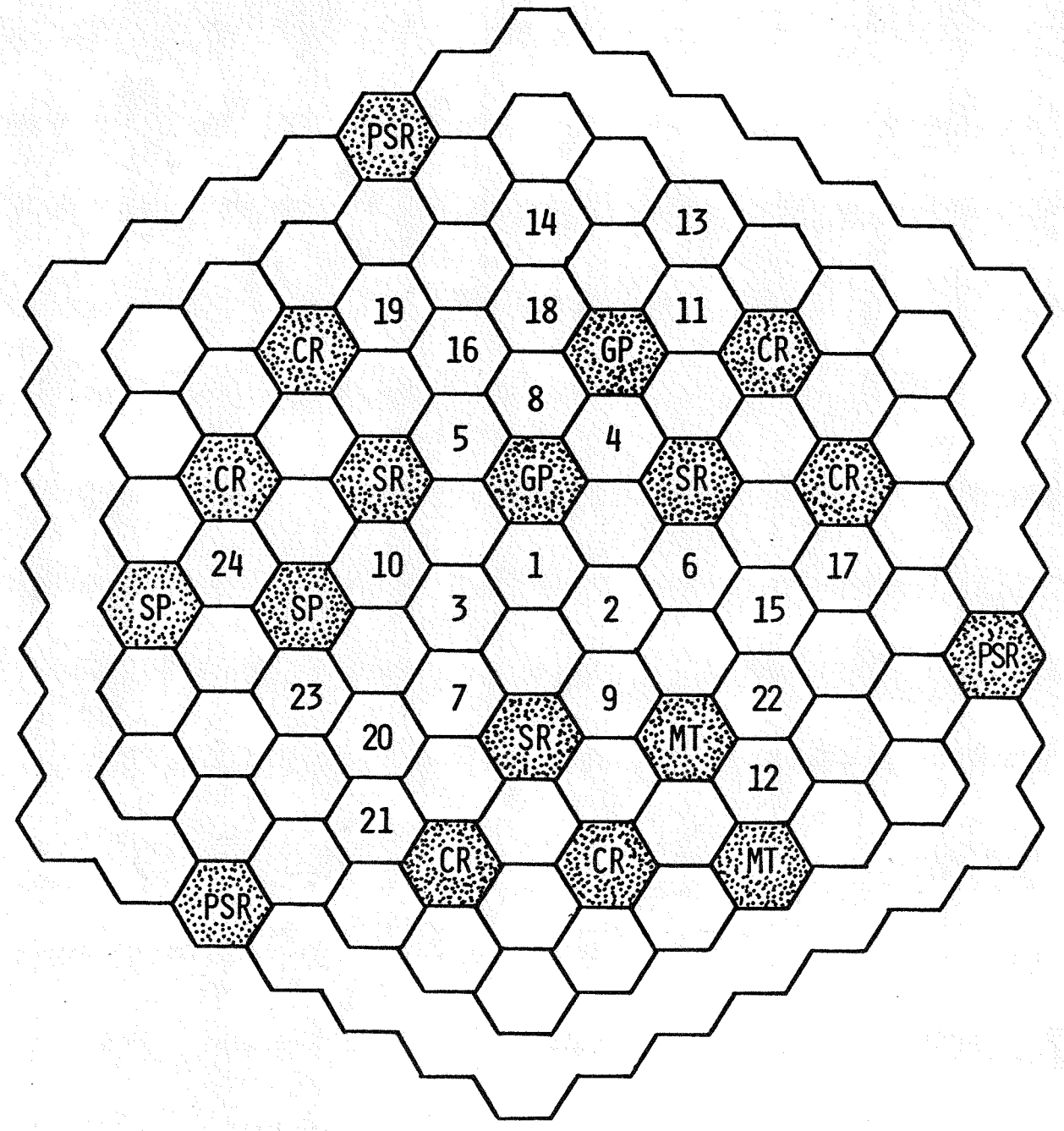

FIGURE 6. BOC-4 Subassembly Failure Sequence (1$/sec TOP)-Failure Potential Model.

HEDL P00422-21

LEGEND

SR	SAFETY ROD
CR	CONTROL ROD
MT	MATERIAL TEST
SP	SPECIAL PURPOSE TEST
GP	GENERAL PURPOSE CLOSED LOOP TEST
PSR	PERIPHERAL SHIM ROD
NN	FAILURE SEQUENCE

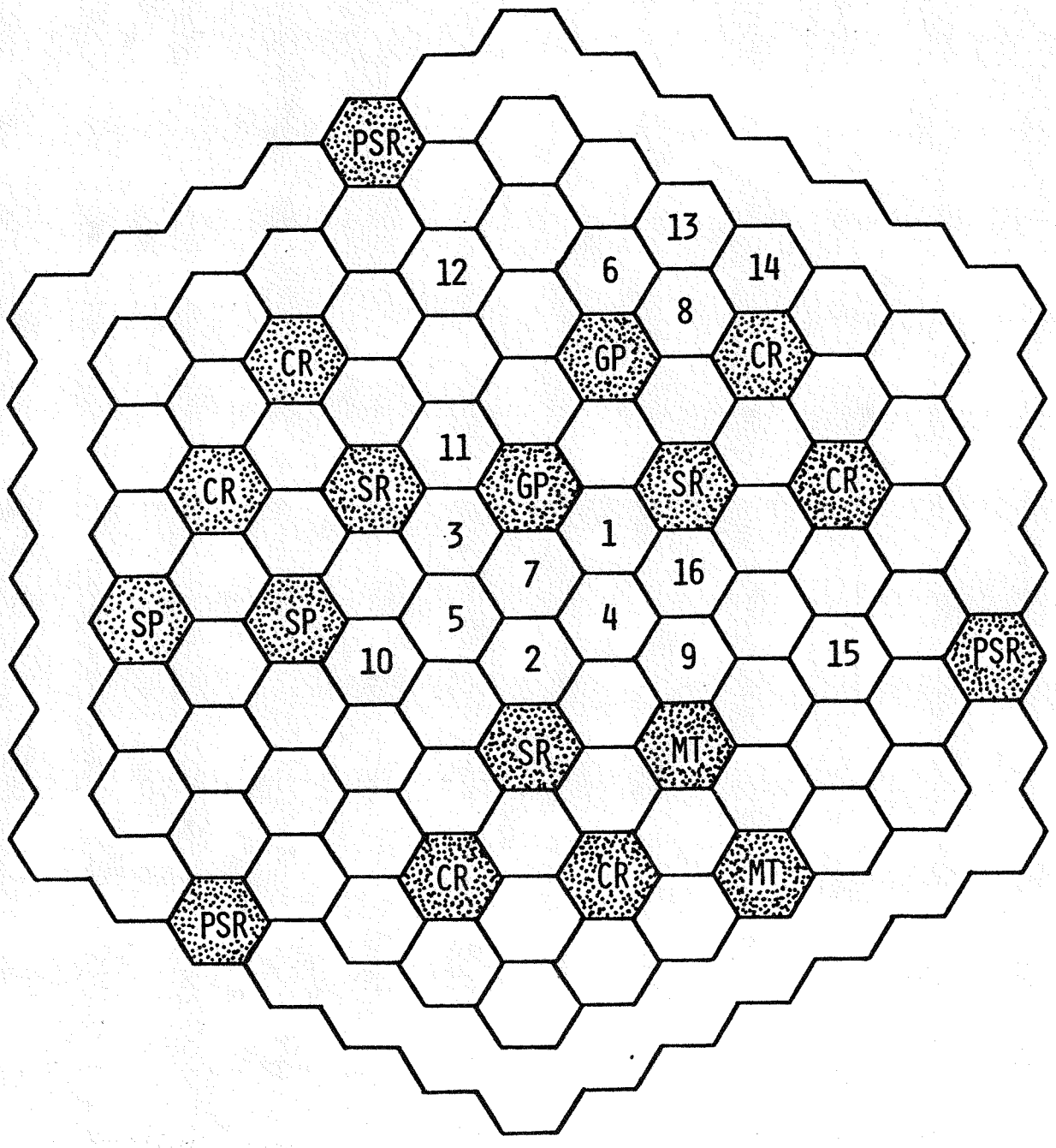

FIGURE 7. EOC-4 Subassembly Failure Sequence (0.5$/sec TOP)-Failure Potential Model.

HEDL P00422-10

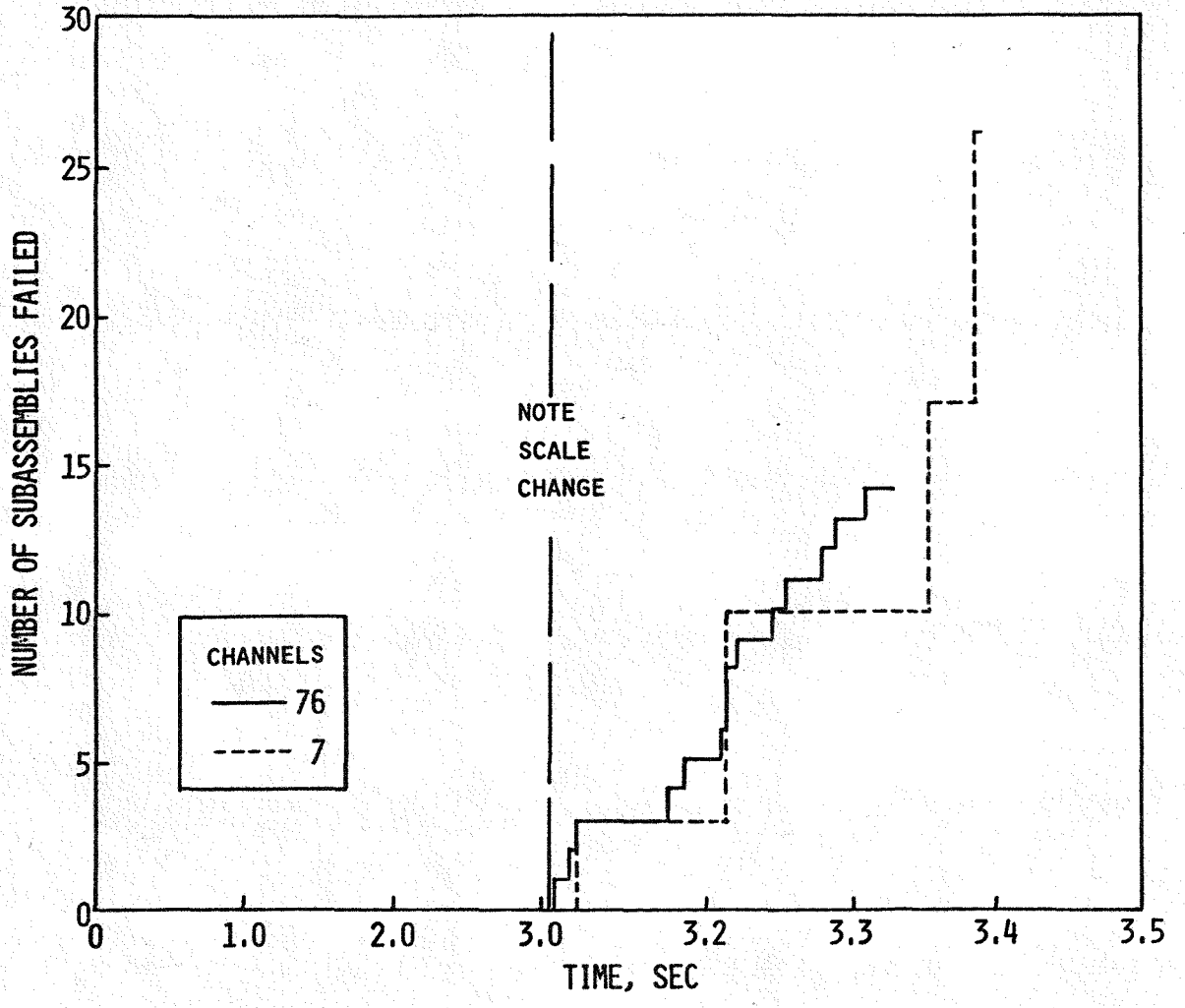

FIGURE 8. BOC-4 Subassemblies Failed vs. Time (0.5$/sec TOP) 76 vs 7 Channels, Failure Potential Model.

HEDL P00422-18

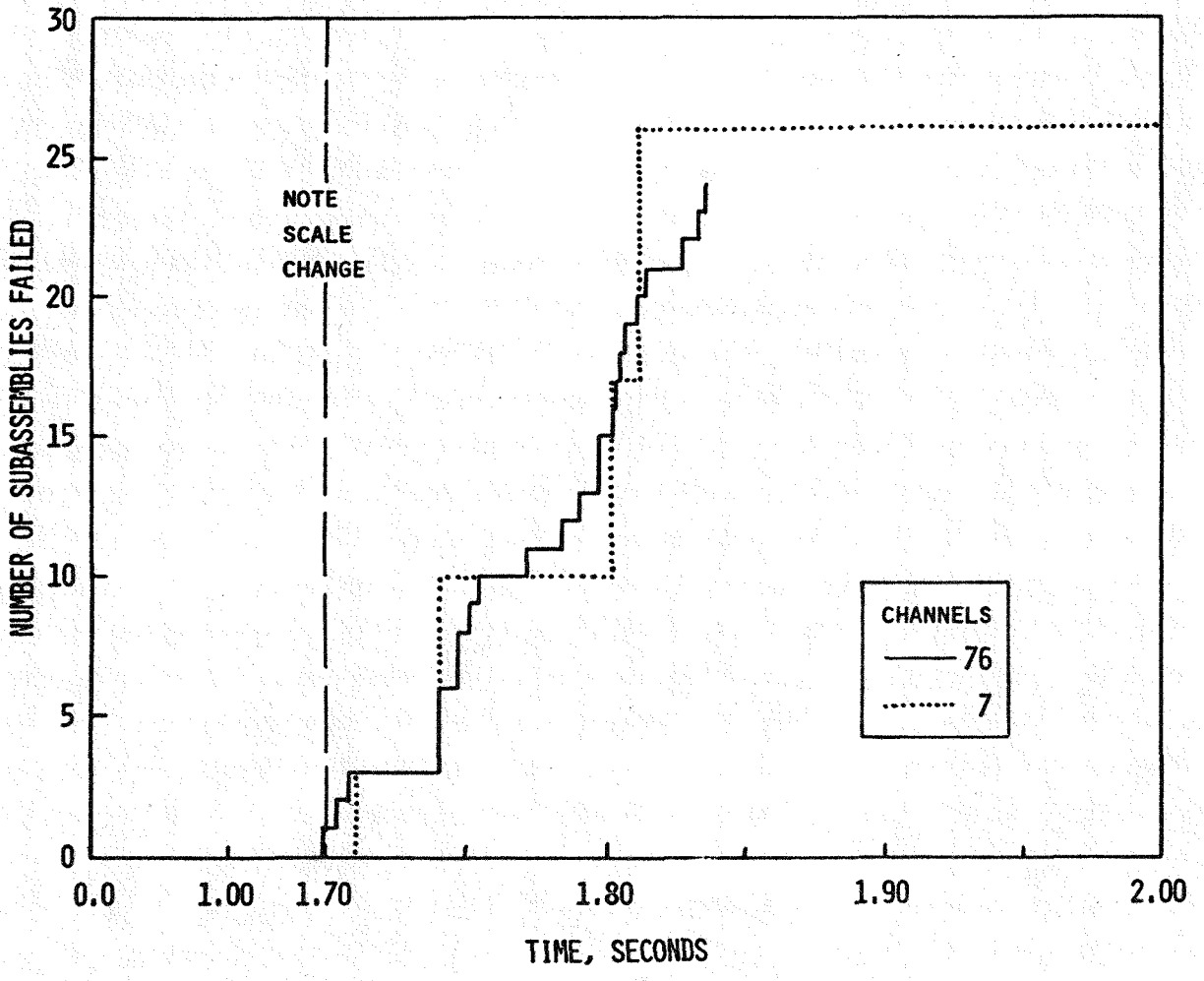

FIGURE 9. BOC-4 Subassemblies Failed vs. Time (1$/sec TOP) 76 vs. 7 Channels, Failure Potential Model.

HEDL P00422-5

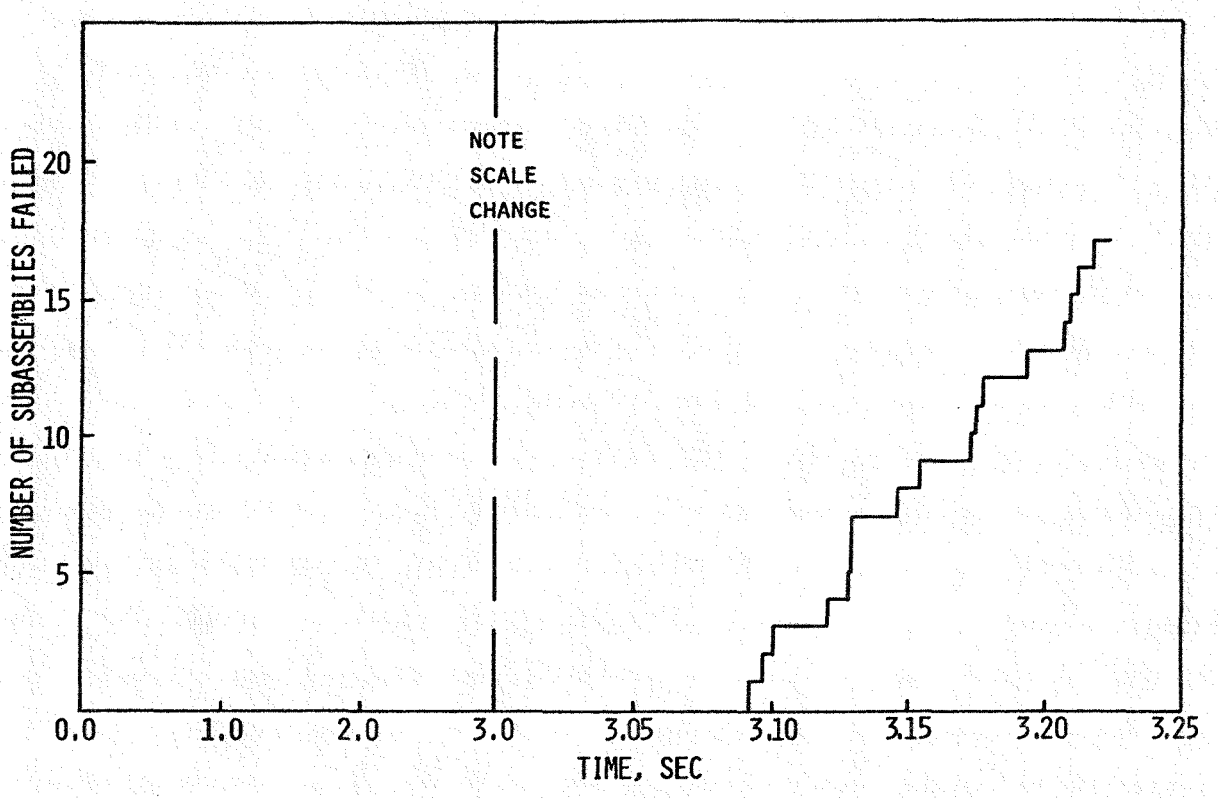

FIGURE 10. EOC-4 Subassemblies Failed vs. Time (0.5$/sec TOP) 76 Channels, Failure Potential Model.

HEDL P00422-12

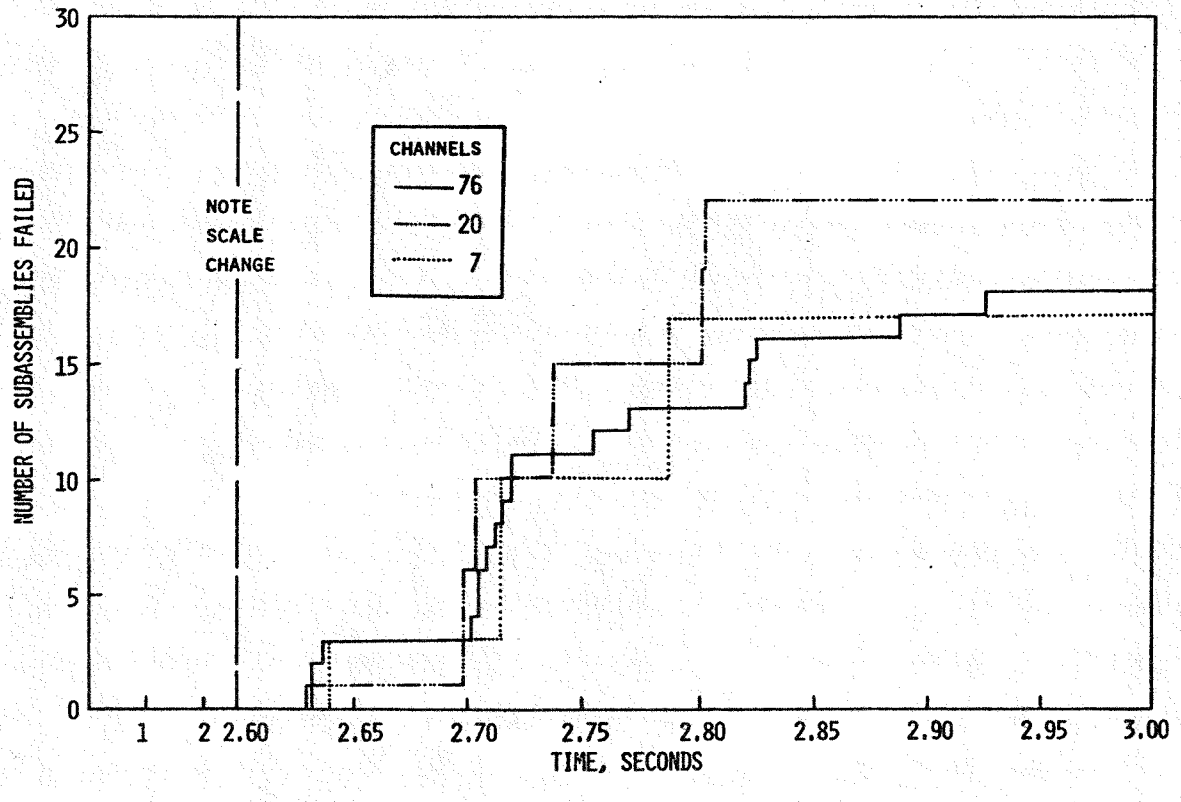

FIGURE 11. BOC-4 Subassemblies Failed vs. Time (0.5$/sec TOP) 76 vs. 20 (Reference 7 Grouping) and 7 channels, Damage Parameter Model. HEDL P00422-20

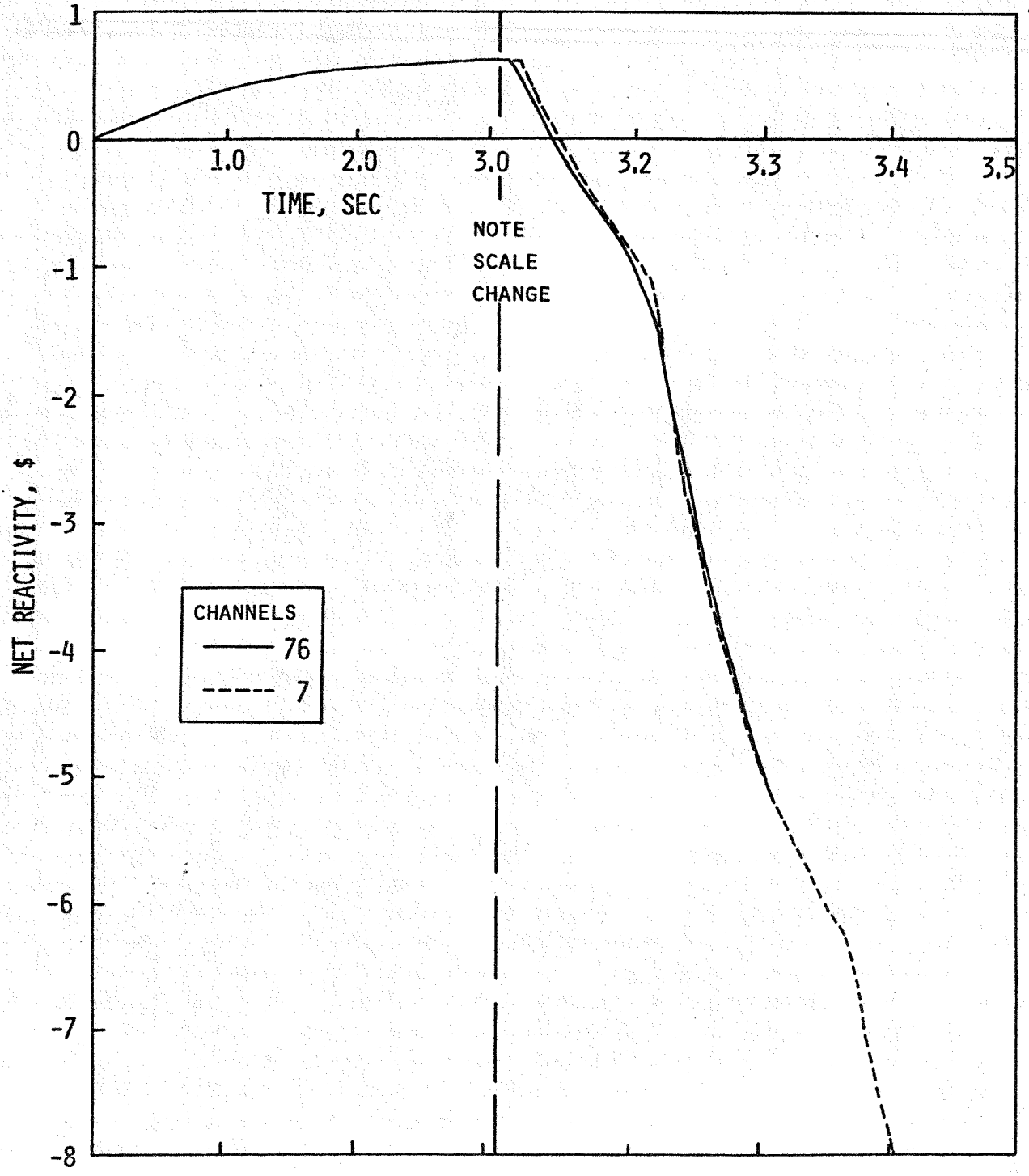

FIGURE 12. BOC-4 Net Reactivity vs. Time (0.5$/sec TOP) 76 vs. 7 Channels, Failure Potential Model. HEDL P00625-8

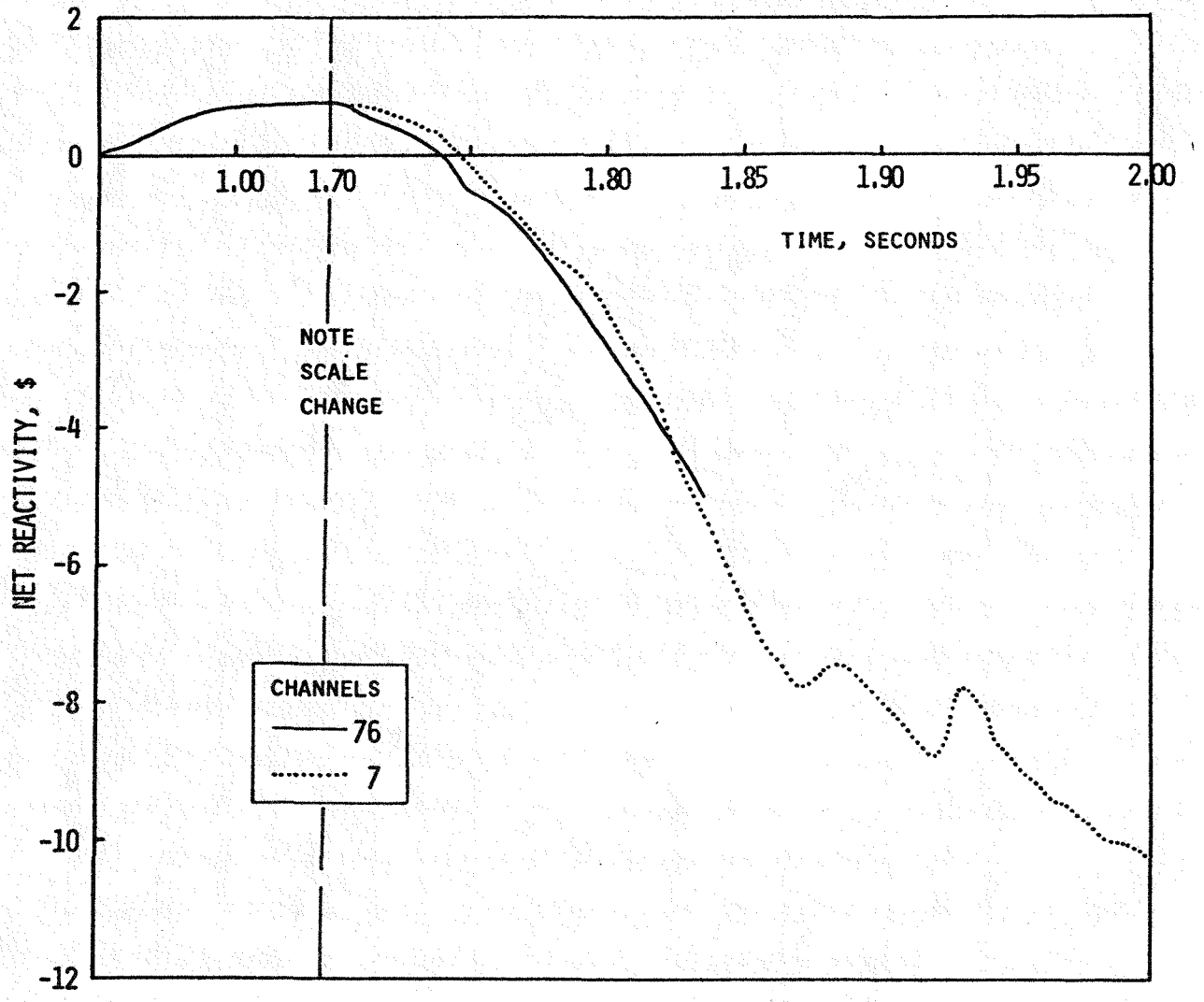

FIGURE 13. BOC-4 Net Reactivity vs. Time (1$/sec TOP) HEDL P00422-13
76 vs. 7 Channels, Failure Potential Model.

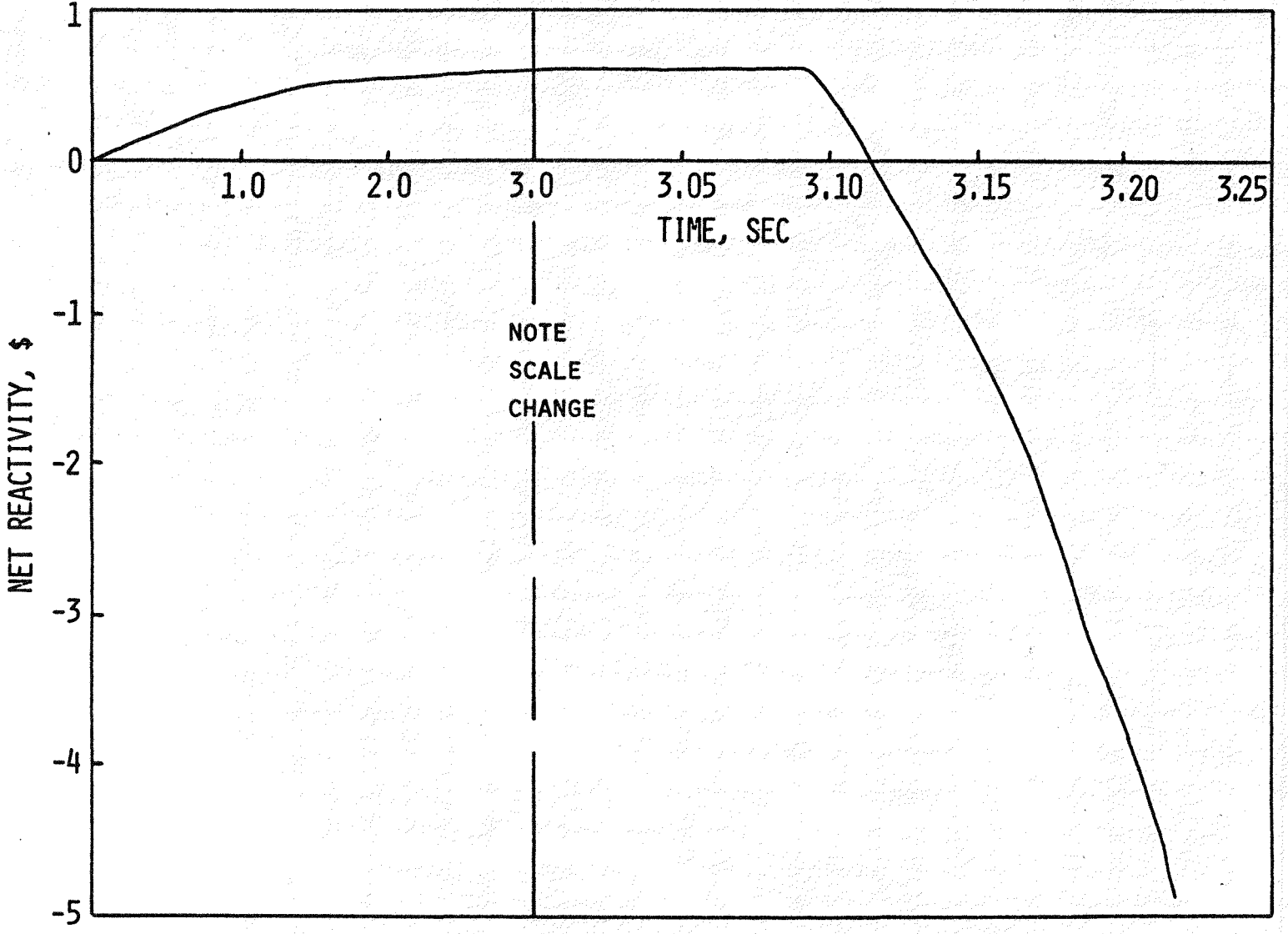

FIGURE 14. EOC-4 Net Reactivity vs. Time (0.5$/sec TOP) 76 Channels, Failure Potential Model.

HEDL P00422-4

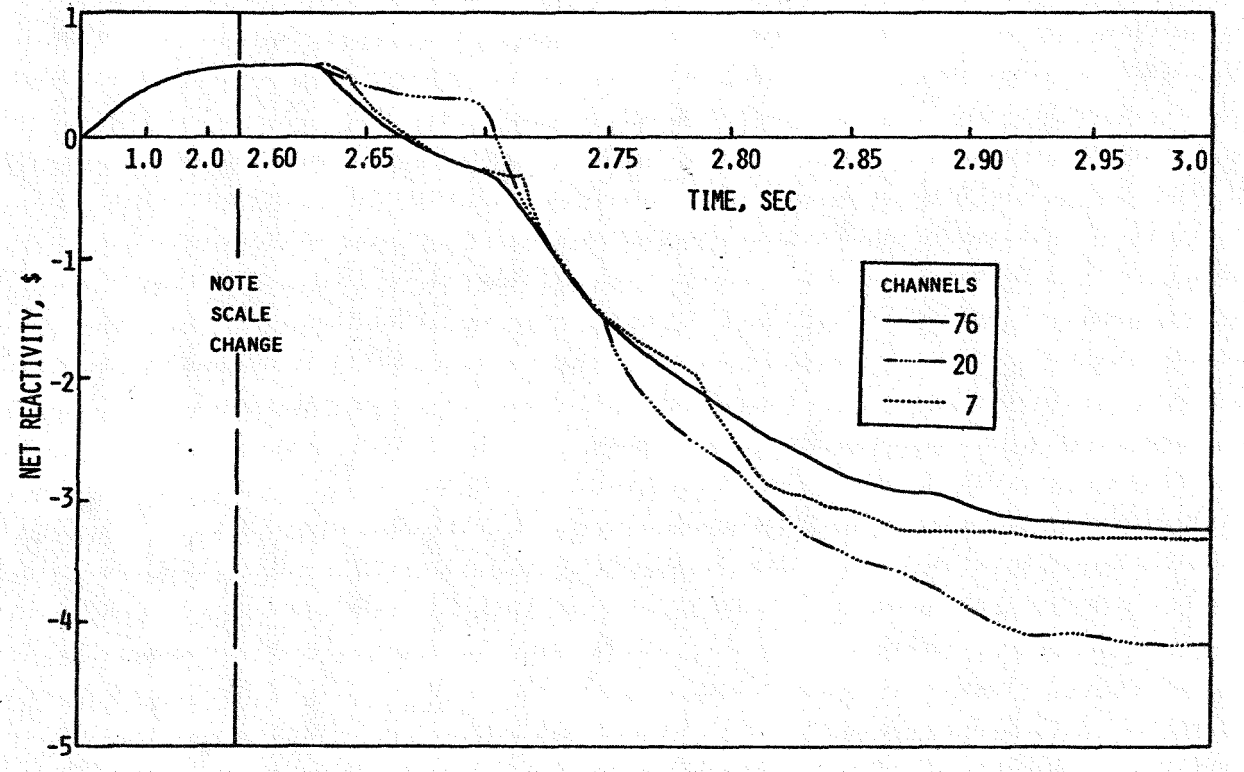

FIGURE 15. BOC-4 Net Reactivity vs. Time (0.5$/sec TOP) HEDL P00422-22
76 vs. 20 (Reference 7 Grouping) and 7 Channels,
Damage Parameter Model.

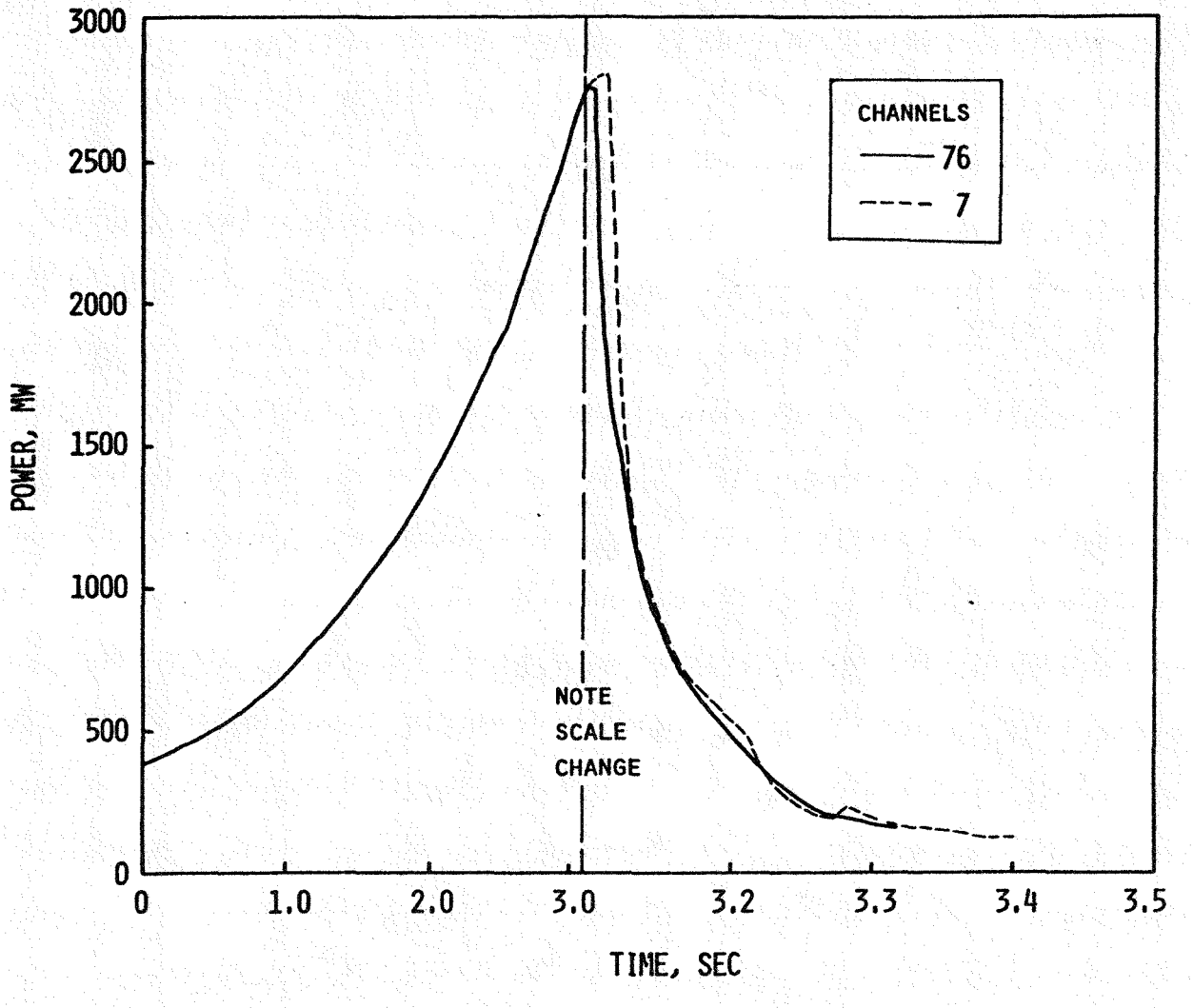

FIGURE 16. BOC-4 Power vs. Time (0.5$/sec TOP) 76 vs. 7 Channels, Failure Potential Model. HEDL P00422-6

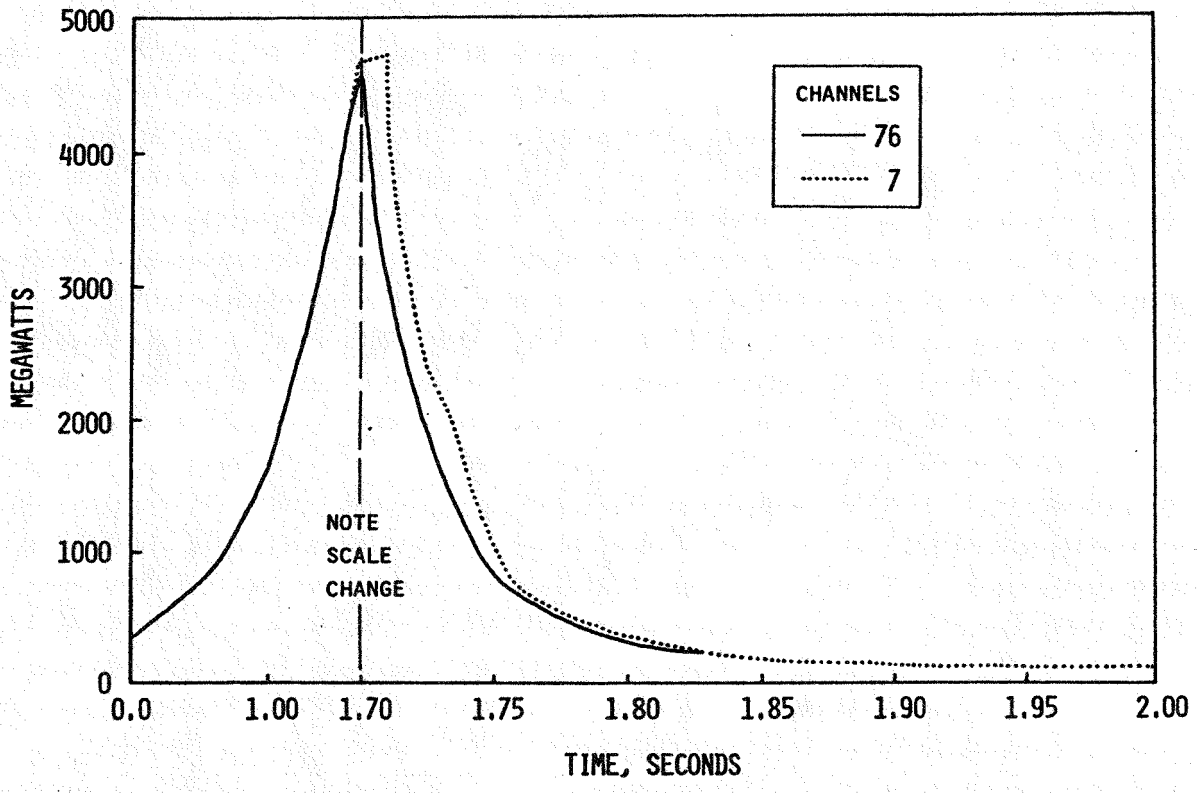

FIGURE 17. BOC-4 Power vs. Time (1$/sec TOP) HEDL P00422-14
76 vs. 7 Channels, Failure Potential Model.

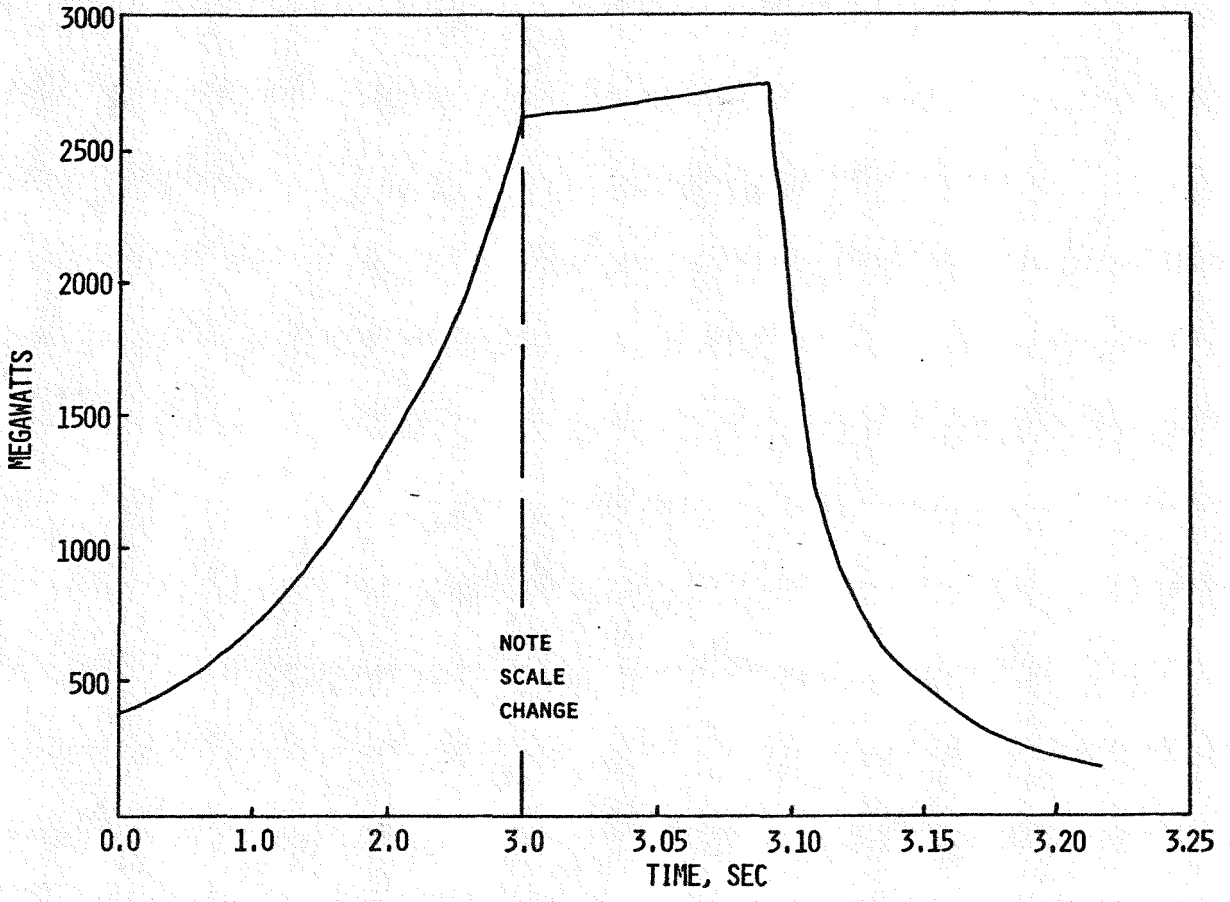

FIGURE 18. EOC-4 Power vs. Time (0.5$/sec TOP) 76 Channels, Failure Potential Model. HEDL P00422-11

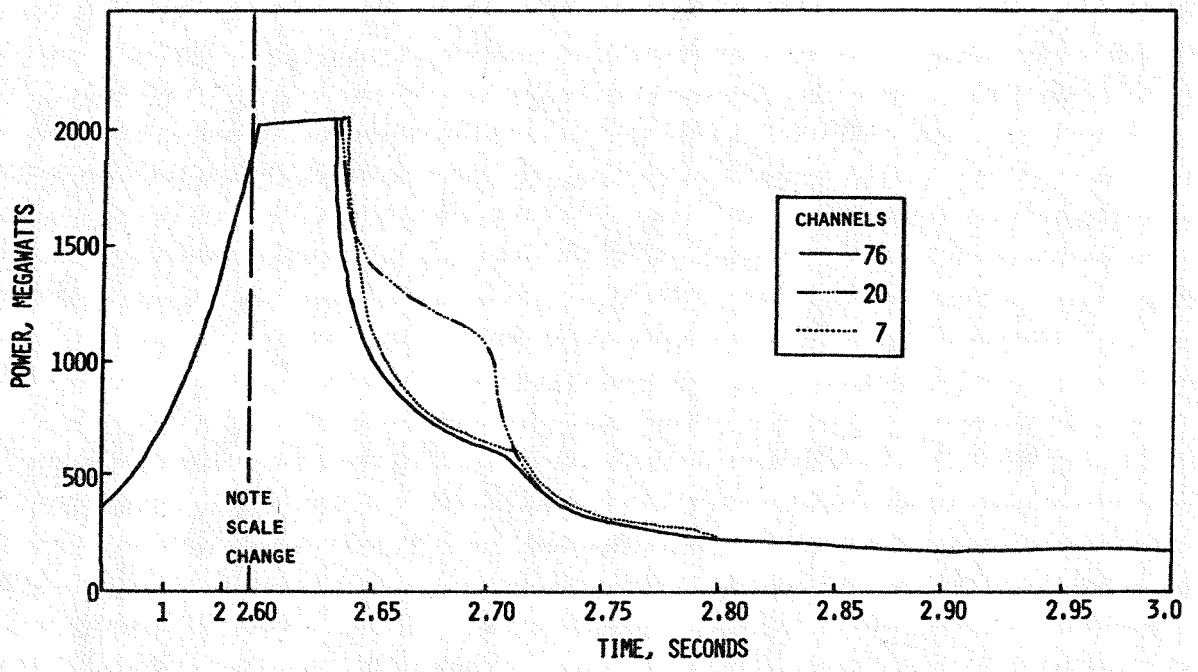

FIGURE 19. BOC-4 Power vs. Time (0.5$/sec TOP) 76 vs. 20 (Reference 7 Grouping) and 7 Channel, Damage Parameter Model. HEDL P00422-15

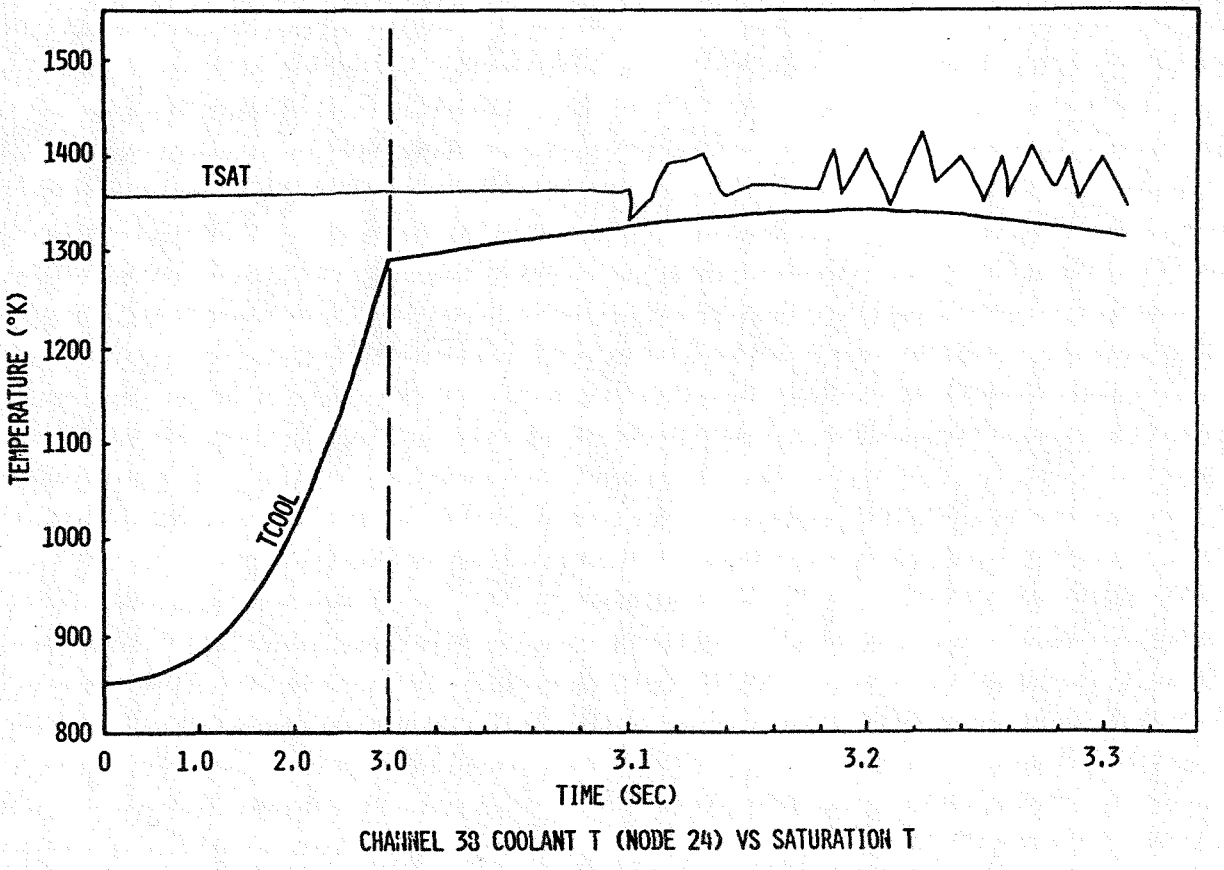

FIGURE 20. Channel 38 Coolant Temperature (Node 24) vs. Saturation Temperature (0.5$/sec TOP). HEDL P00422-3

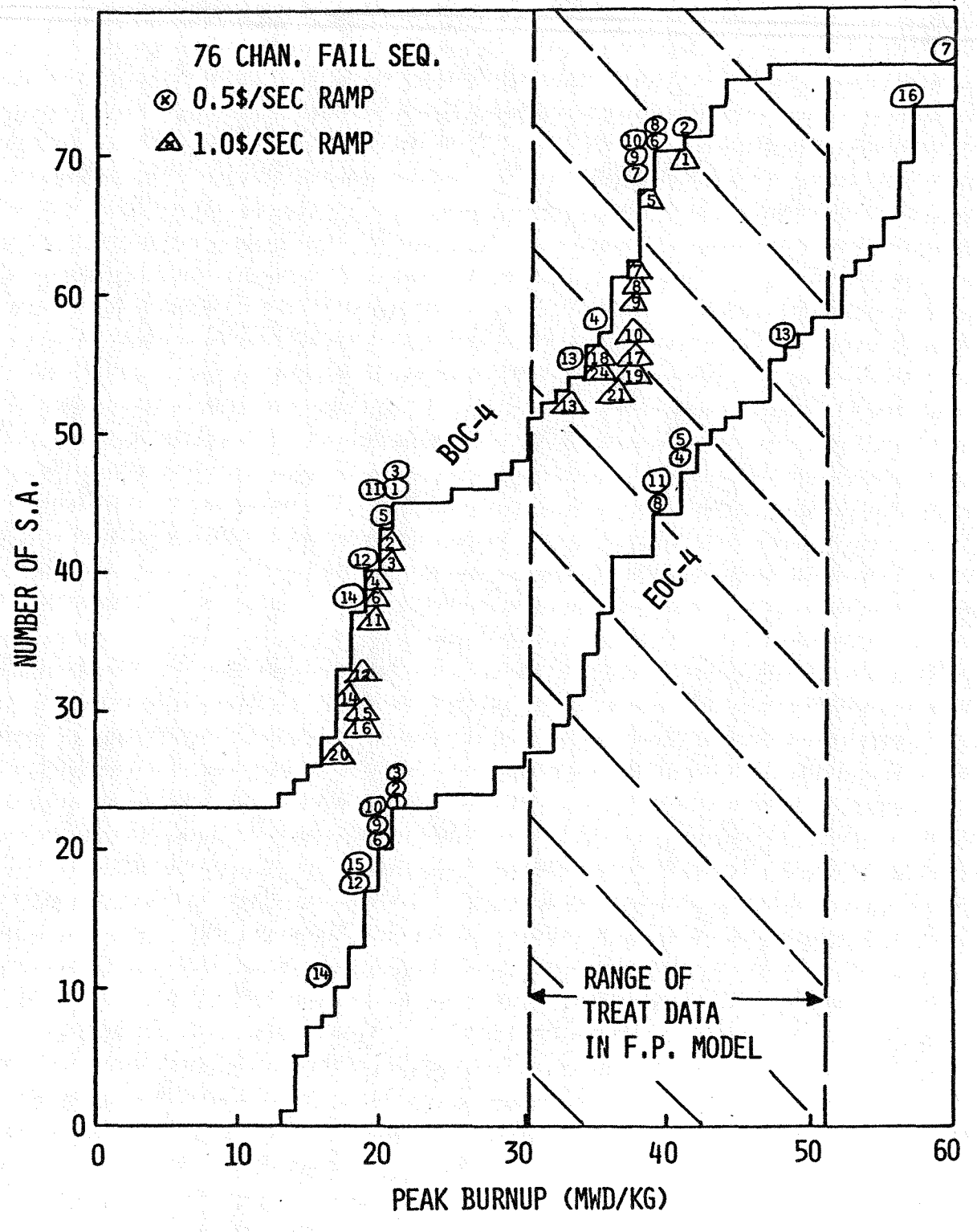

FIGURE 21. 76-Channel Failure Sequences Predicted by Failure Potential Model vs. Burnup.

HEDL P00422-7

LEGEND

SR	SAFETY ROD
CR	CONTROL ROD
MT	MATERIAL TEST
SP	SPECIAL PURPOSE TEST
GP	GENERAL PURPOSE CLOSED LOOP TEST
PSR	PERIPHERAL SHIM ROD
N	7-CHANNEL IDENTIFICATION

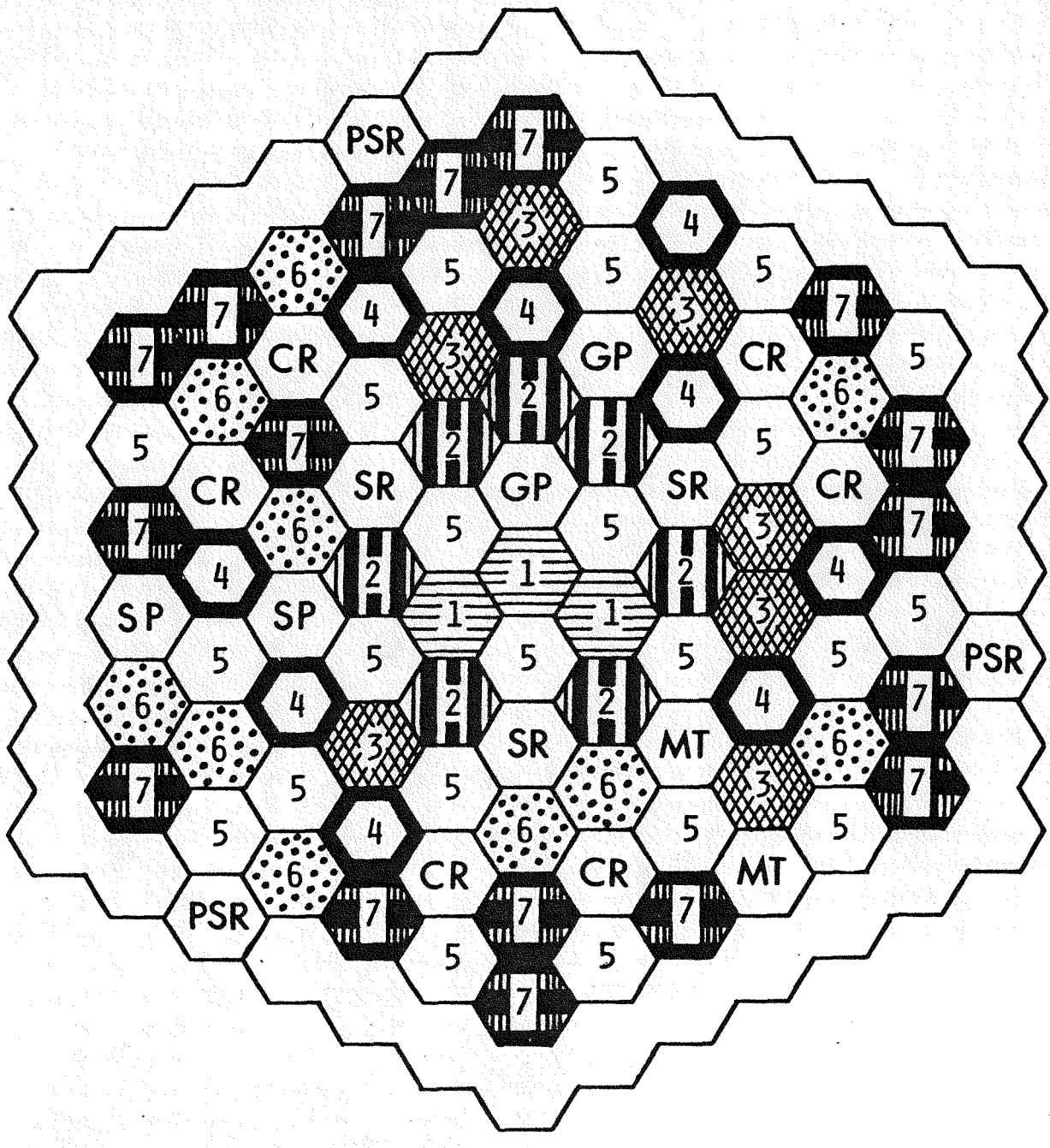

FIGURE 22. BOC-4 Subassembly Grouping for 7 Channels. HEDL P00422-1

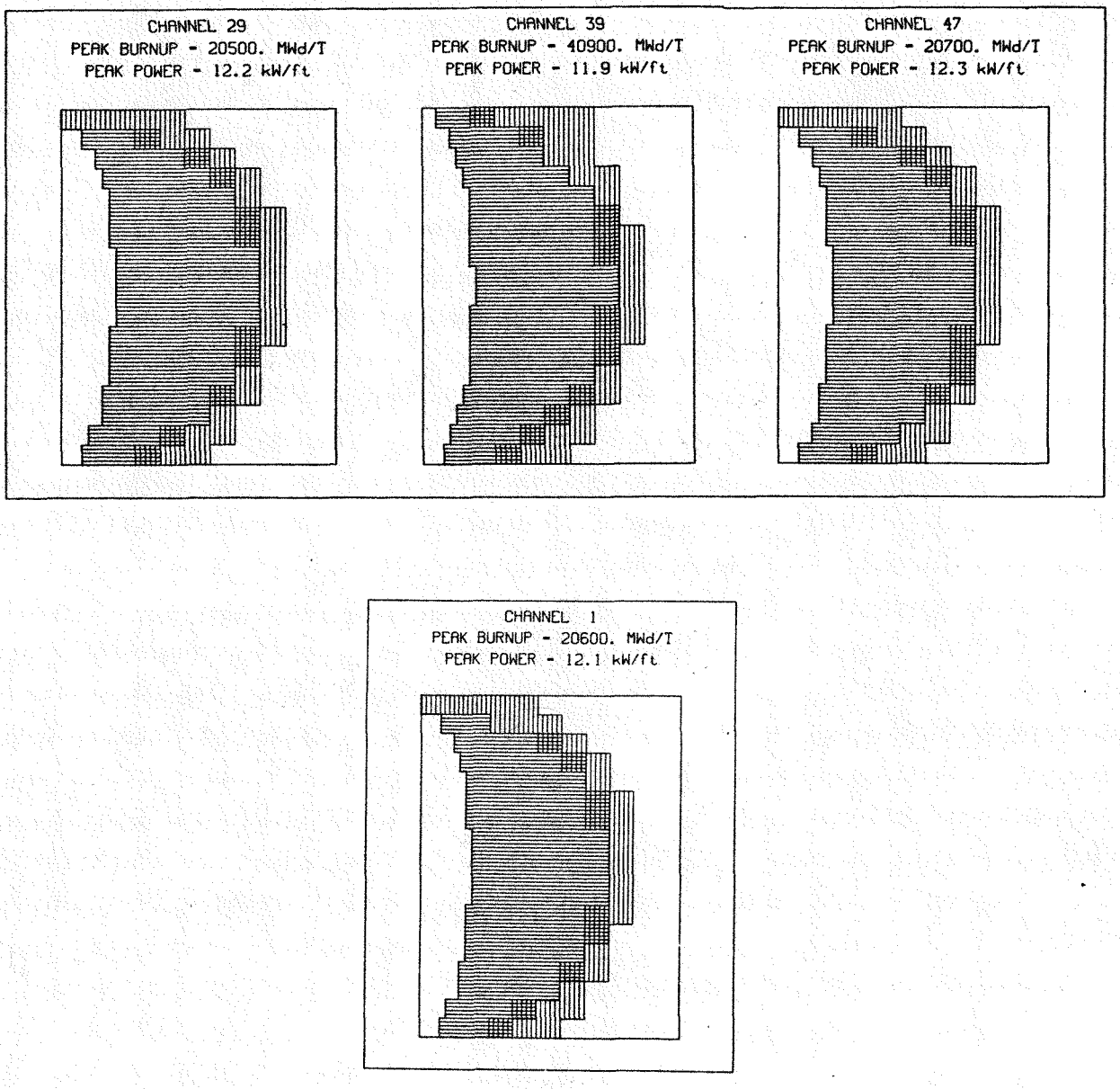

FIGURE 23. Microstructure Variation Between Subassemblies Grouped into Channel 1 of 7 Channels.

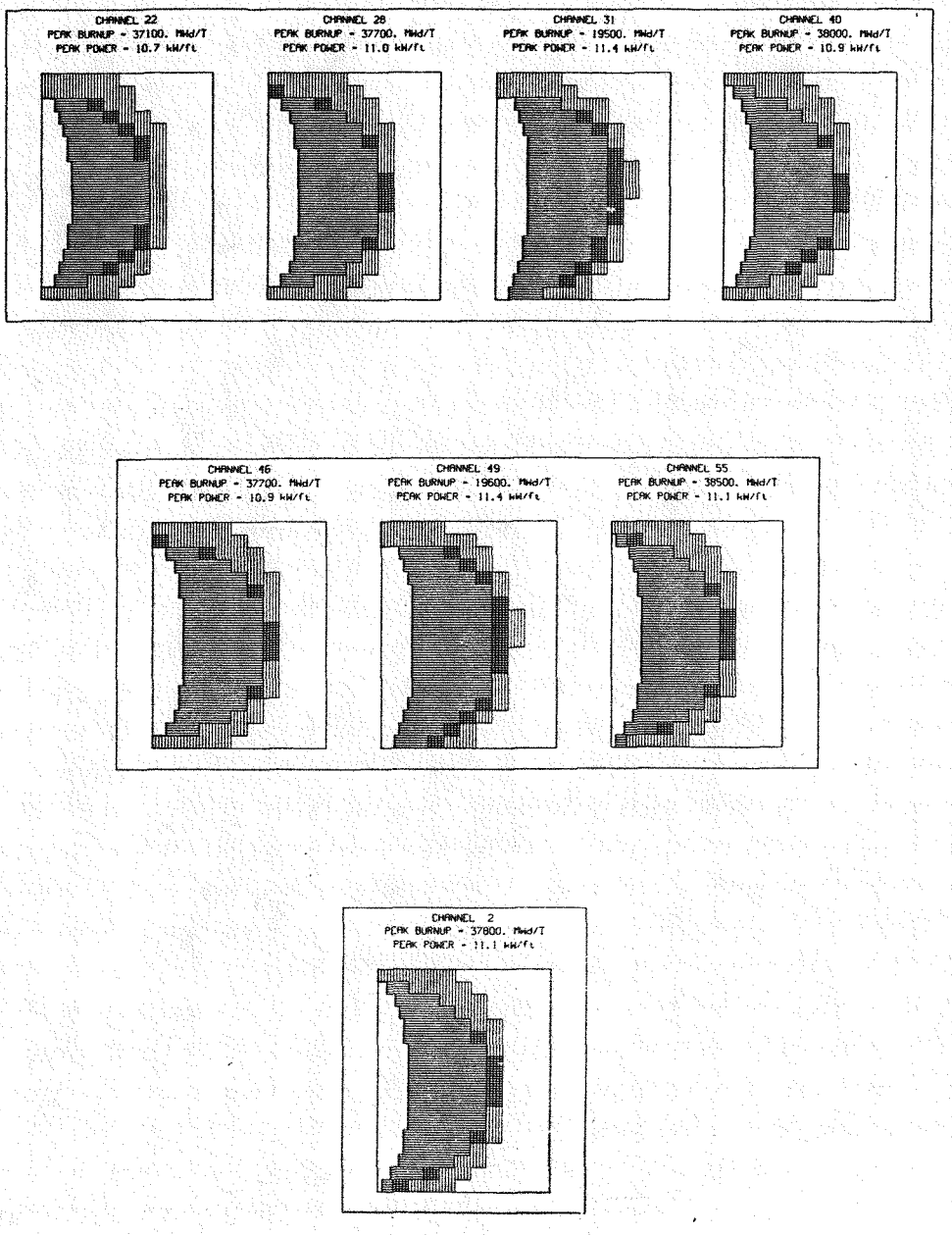

FIGURE 24. Microstructure Variation Between Subassemblies Grouped into Channel 2 of 7 Channels.

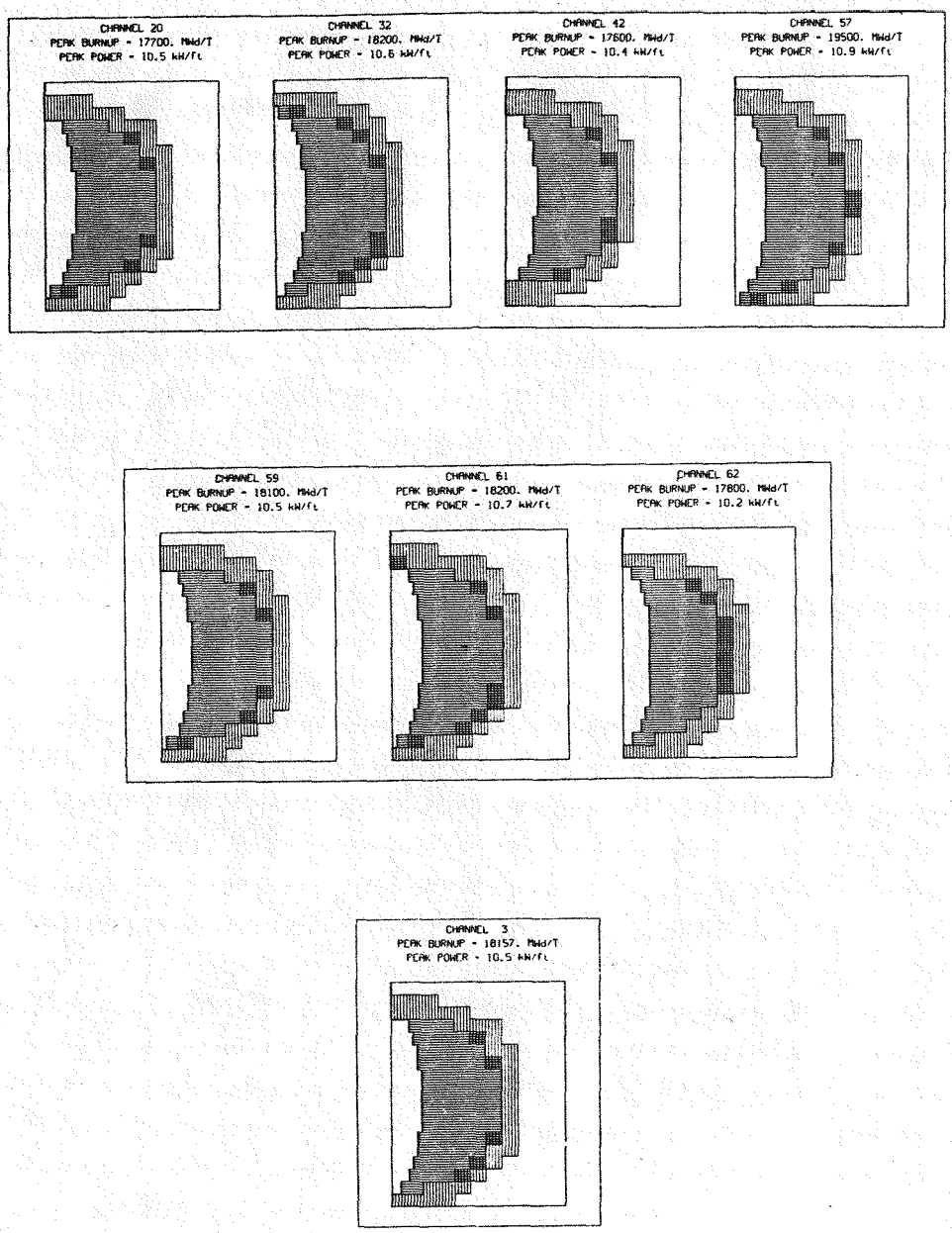

FIGURE 25. Microstructure Variation Between Subassemblies Grouped into Channel 3 of 7 Channels.

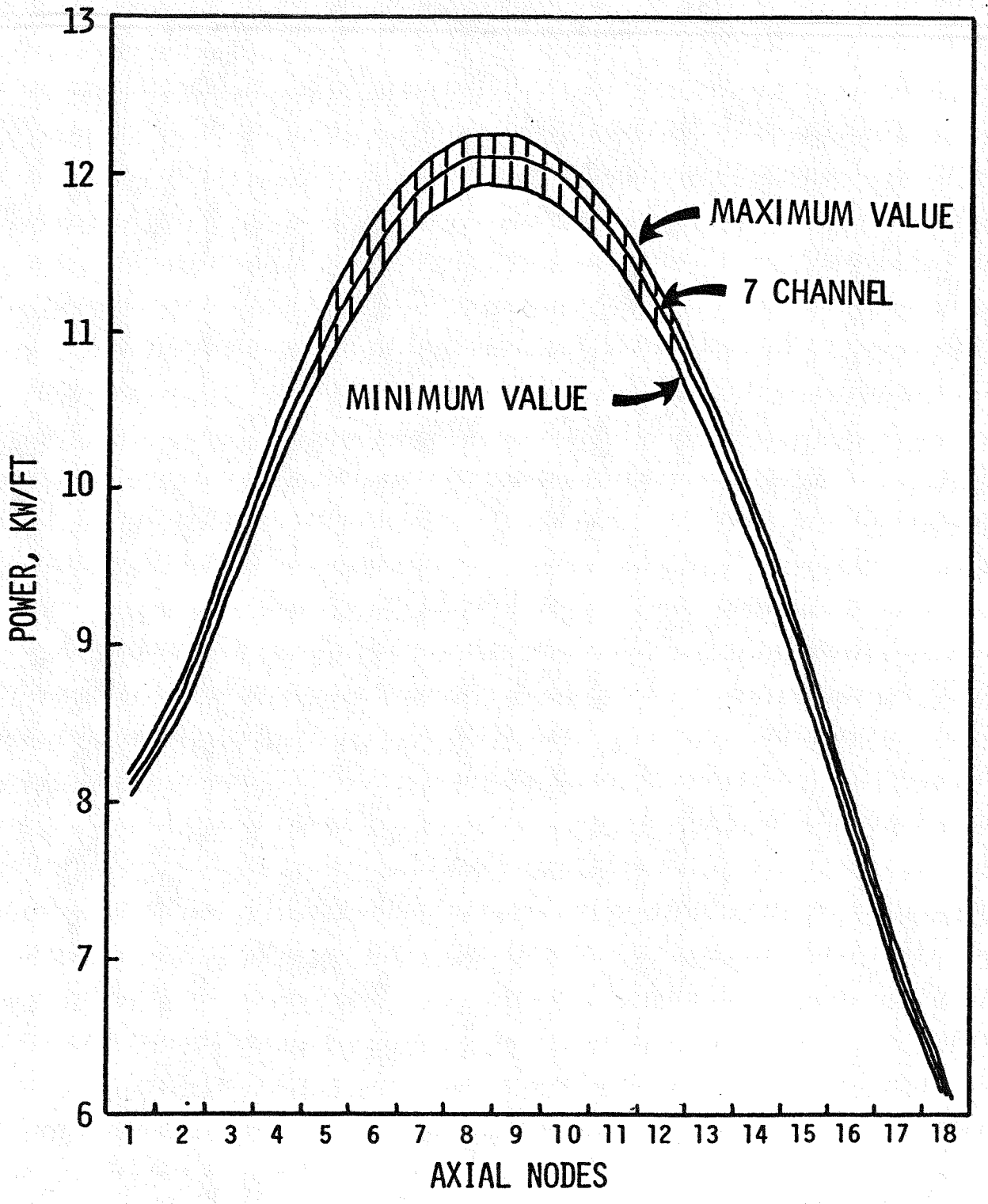

FIGURE 26. Axial Power Profile Variations Between Subassemblies Grouped into Channel 1 of 7 Channels.

HEDL P00422-2

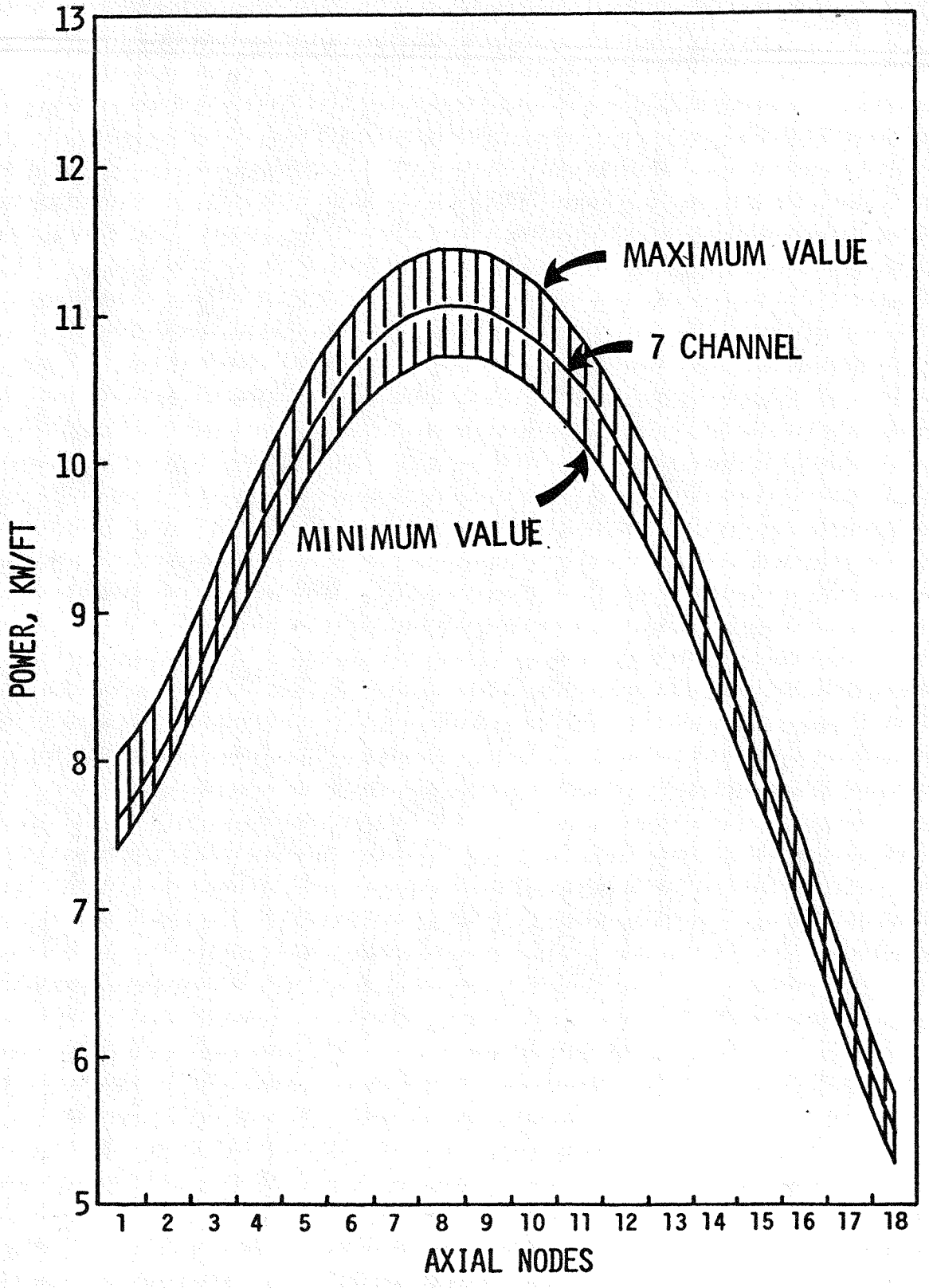

FIGURE 27. Axial Power Profile Variations Between Subassemblies Grouped into Channel 2 of 7 Channels.

HEDL P00422-8

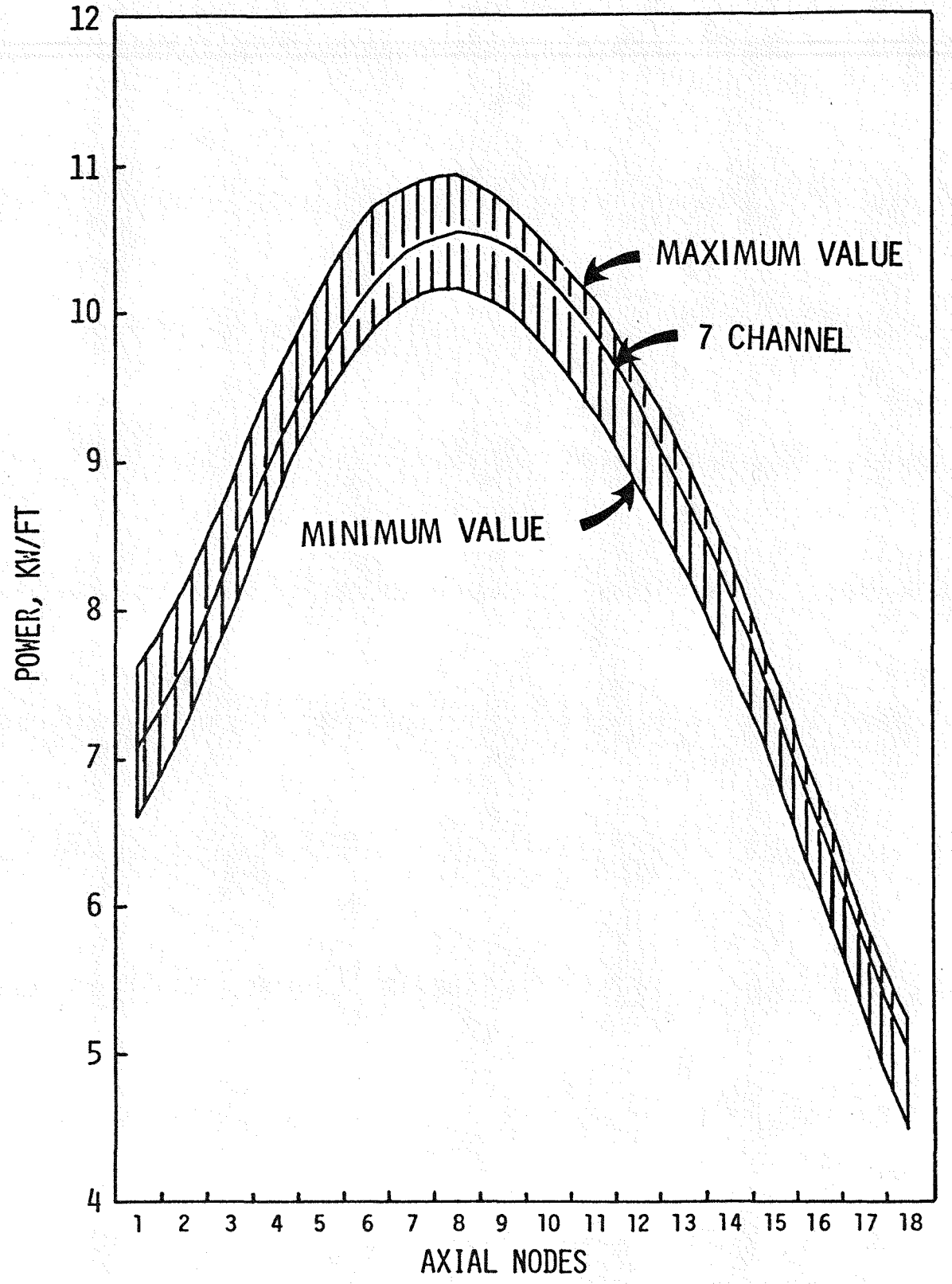

FIGURE 28. Axial Power Profile Variations Between Subassemblies Grouped into Channel 3 of 7 Channels.

HEDL P00422-19